Title

INHOMOGENEOUS ELECTRIC DEFLECTING FIELD FOR ANALYSIS OF ROTATIONAL EXCITATION IN REACTIVE SCATTERING OF MOLECULAR BEAMS

Authors

Herm, Ronald R.
Herschbach, Dudley R.

Publication Date

1965-07-01

UCRL-16039

University of California

Ernest O. Lawrence Radiation Laboratory

INHOMOGENEOUS ELECTRIC DEFLECTING FIELD FOR ANALYSIS OF ROTATIONAL EXCITATION IN REACTIVE SCATTERING OF MOLECULAR BEAMS

Berkeley, California

DISCLAIMER

Submitted for publi. in Journal of
Chemical Physics.

UCRL-16039

UNIVERSITY OF CALIFORNIA

Lawrence Radiation Laboratory
Berkeley, California

AEC Contract No. W-7405-eng-48

INHOMOGENEOUS ELECTRIC DEFLECTING FIELD FOR ANALYSIS OF ROTATIONAL EXCITATION IN REACTIVE SCATTERING OF MOLECULAR BEAMS

Ronald R. Herm and Dudley R. Herschbach

July 1965

TABLE OF CONTENTS

UCRL-16039

INHOMOGENEOUS ELECTRIC DEFLECTING FIELD FOR ANALYSIS OF ROTATIONAL EXCITATION IN REACTIVE SCATTERING OF MOLECULAR BEAMS*

Ronald R. Herm[†‡] and Dudley R. Herschbach[‡]

Department of Chemistry and Lawrence Radiation Laboratory
University of California, Berkeley, California 94720

Abstract

An inhomogeneous electric field producing a "congruent two-wire" electric field in the gap between the electrodes has been constructed. The field is six inches long, with a maximum distance across the gap of 0.125 inches, and is powered by a DC voltage supply variable from zero to fifty kilovolts. The strength of the field is such that an effective dipole of 0.005 Debye traveling with thermal energy (~500°K) will experience a measurable deflection upon traversing the field. The deflecting field has been incorporated into a molecular beam scattering apparatus designed to analyze for rotational excitation in the product of a chemical reaction. The deflection of thermal beams of cesium atoms and of cesium chloride molecules upon traversing the field has been measured, and the observed deflection patterns agree well with those predicted theoretically.

---

*Support received from the U. S. Atomic Energy Commission and the Alfred P. Sloan Foundation is gratefully acknowledged.

†National Science Foundation Predoctoral Fellow, 1961-65.

‡Present address: Department of Chemistry, Harvard University, Cambridge, Massachusetts 02138.

INTRODUCTION

In an electric field $\underset{\sim}{E}$ a neutral molecule possessing a constant dipole moment component in the direction of the field, μ_e, and independent of the strength of the field will experience a Stark effect energy shift given by

$$W_e = -\mu_e E.$$

Since the dependence of W_e on position is determined by the spatial inhomogeneity of the field, the molecule will be subject to a force

$$\underset{\sim}{F} = \mu_e \underset{\sim}{\nabla} E. \tag{1}$$

In the general case the dependence of W_e on E may be more complicated. However, the force may still be expressed as in Eq. (1) where μ_e, the effective dipole moment, is given by

$$\mu_e = -\partial W_e / \partial E. \tag{2}$$

As an atom or molecule will interact with an inhomogeneous electric field either through a permanent or an induced dipole moment, it will experience a transverse deflection upon traversing the field which will depend on the field inhomogeneity and on its velocity and internal quantum state. A beam of atoms or nonpolar molecules will be deflected by virtue of a field induced dipole moment arising from the polarizability interaction; this will always result in a deflection

toward the region of high field strength. A polar diatomic molecule will be deflected in the field as a result of the interaction between its permanent dipole moment and the field. Both the magnitude and sign of the resulting effective dipole moment, Eq. (2), will depend on the total angular momentum of the molecule, J, and its projection on the field direction, M_J.

Inhomogeneous electric fields have been a valuable tool in molecular beam studies of isolated atoms and molecules, especially in connection with electric resonance studies of molecular properties;[1-3] however, little use of such fields has yet been made in connection with beam studies of collisions between atoms and molecules. Recently, Bennewitz et al.[4] have employed an electric quadrupole focussing field to compare the total cross sections for beams of thallous fluoride (TlF) in the (1,0) and (1,1) rotational states scattered by rare gas atoms. Kramer and Bernstein[5] have also recently employed a six-pole electric field to refocus states of polar symmetric top molecules (which exhibit a first order Stark effect) with the same negative dipole moment component with respect to the field direction.

This report describes the construction of an inhomogeneous electric field and auxilary apparatus to be used in molecular beam scattering experiments. The apparatus is designed to determine the rotational distribution in product MX molecules formed in chemical reactions of the type

$$M + RX \rightarrow MX + R \qquad (3)$$

where M is an alkali atom, X a halogen atom, and R some arbitrary

chemical group. The apparatus was constructed at Berkeley and later moved to Harvard. A preliminary deflection experiment on a thermal potassium atom beam was performed at Berkeley.[6] In addition, deflection patterns of thermal beams of cesium and of cesium chloride which were measured at Harvard are described in this report. Successful measurements of the rotational distribution of reactively scattered alkali halide molecules have also been made at Harvard and are described elsewhere.[7]

Angular Momentum in Chemical Reactions

In the notation adopted in this report, the orbital angular momentum of approach of the reactant molecules will be denoted by $\underset{\sim}{L}$, that of departure of the products by $\underset{\sim}{L}'$, and the rotational angular momenta of RX, MX, and R by $\underset{\sim}{J}$, $\underset{\sim}{J}'$, and $\underset{\sim}{J}''$ respectively. Angular momentum conservation requires that

$$\underset{\sim}{L} + \underset{\sim}{J} = \underset{\sim}{F} = \underset{\sim}{L}' + \underset{\sim}{J}' + \underset{\sim}{J}'' \tag{4a}$$

where $\underset{\sim}{F}$ is the total angular momentum of the collision and any electronic or nuclear spins are neglected. Angular momentum conservation further implies that the projections of these various momenta in the direction of the field be related by

$$M_L + M_J = M_F = M_L' + M_J' + M_J''. \tag{4b}$$

Theoretical studies have indicated that, under certain conditions, nearly all of the orbital angular momenta of the reactants should appear as rotation in the MX product.[8-11] Such a partitioning of angular momenta in the reaction would imply strong polarization in $\underset{\sim}{J}'$, with $\underset{\sim}{J}'$ approximately confined to a plane orthogonal to the relative velocity vector of the reactants. As will be apparent later in this report, the

breadth of a beam of product alkali halides deflected by the field should be sensitive to the magnitude of J' while the asymmetry of the deflection pattern will reflect the distribution in M_J' and indicate whether polarization is present.

General Design Considerations

Inhomogeneous deflecting fields may be classified as diverging or refocussing fields. A diverging field has the property that the force exerted on a particle will always be in one direction, regardless of the particle's transit time through the field; thus, this field will always broaden a beam which traverses it. Alternatively, by choosing a field configuration of cylindrical symmetry such that the force acting on a beam particle is always directly radially and is proportional to its distance from the symmetry axis, those beam trajectories for which the force is directed radially inward will execute simple harmonic motion. Such particles radiating from a point source will be refocussed at some point along the field axis. The focal length will depend on the field strength and the velocity and effective dipole moment of the particles.[12]

To date, such fields have been used to refocus particles exhibiting first or second order Stark effects. The fields have employed electrode configurations consisting of either six (for first order Stark effects) or four (for second order) rods symmetrically placed and charged. However, it might be possible to achieve the same focussing effect with one charged rod in conjunction with a grounded electrode of appropriate symmetry such that the charged rod and its image charges produce the desired cylindrical symmetry. This technique has already

been used in mass spectroscopy[13] to simulate the action of a four-pole field[14] by means of a monopole.

The field we have constructed is of the traditional "two-wire" diverging design. The choice of a diverging field as opposed to a refocussing one was determined by the nature of the proposed experiment. As the rotational distribution in product MX molecule is to be determined, very high rotational states will probably be populated (on the order of 100 to 200 $\hbar$). Focussing fields, however, will efficiently focus only very low rotational states. This low efficiency toward refocussing high rotational states arises because they correspond to very small effective dipole moments ($0.25 - 1.0 \times 10^{-3}$ Debyes); consequently, an extremely long field would be required to refocus them. In addition, for these high rotational states, the polarizability interaction, which is always diverging, may become comparable to the weak refocussing dipole interaction.

Finally, to complete the summary of deflecting electric fields, it should be pointed out that the "two-wire" design we have chosen, while possessing many desirable characteristics described later in this report, does produce a force which is strongly dependent on the position of the particle within the field. By employing a different design for the electrodes, it is possible to produce a diverging field with the property that the force exerted on a particle traversing it is independent of the particle's position with the field.[15]

An idea of the strength of the field we have constructed may be inferred from Figs. 1 and 2. The deflections plotted were calculated for an applied potential, V_o, of 30 kv. However, these figures can

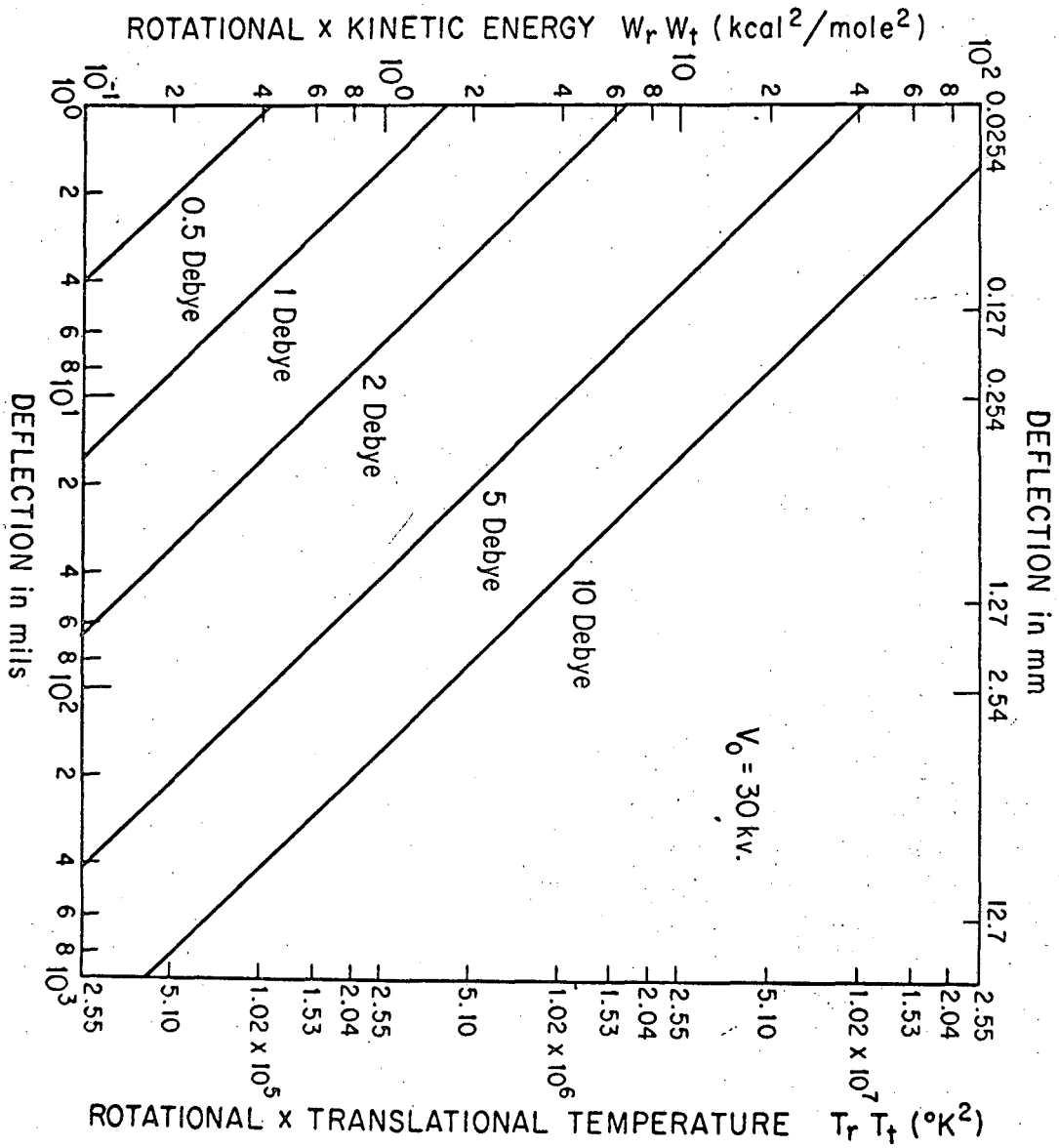

Fig. 1. Deflecting power of field at thirty kilovolts. The deflection of a rotating dipole with $|M_J| = J$ is plotted. The right-hand ordinate gives the result for a thermal distribution of such dipoles with both translational and rotational velocities equal to kT.

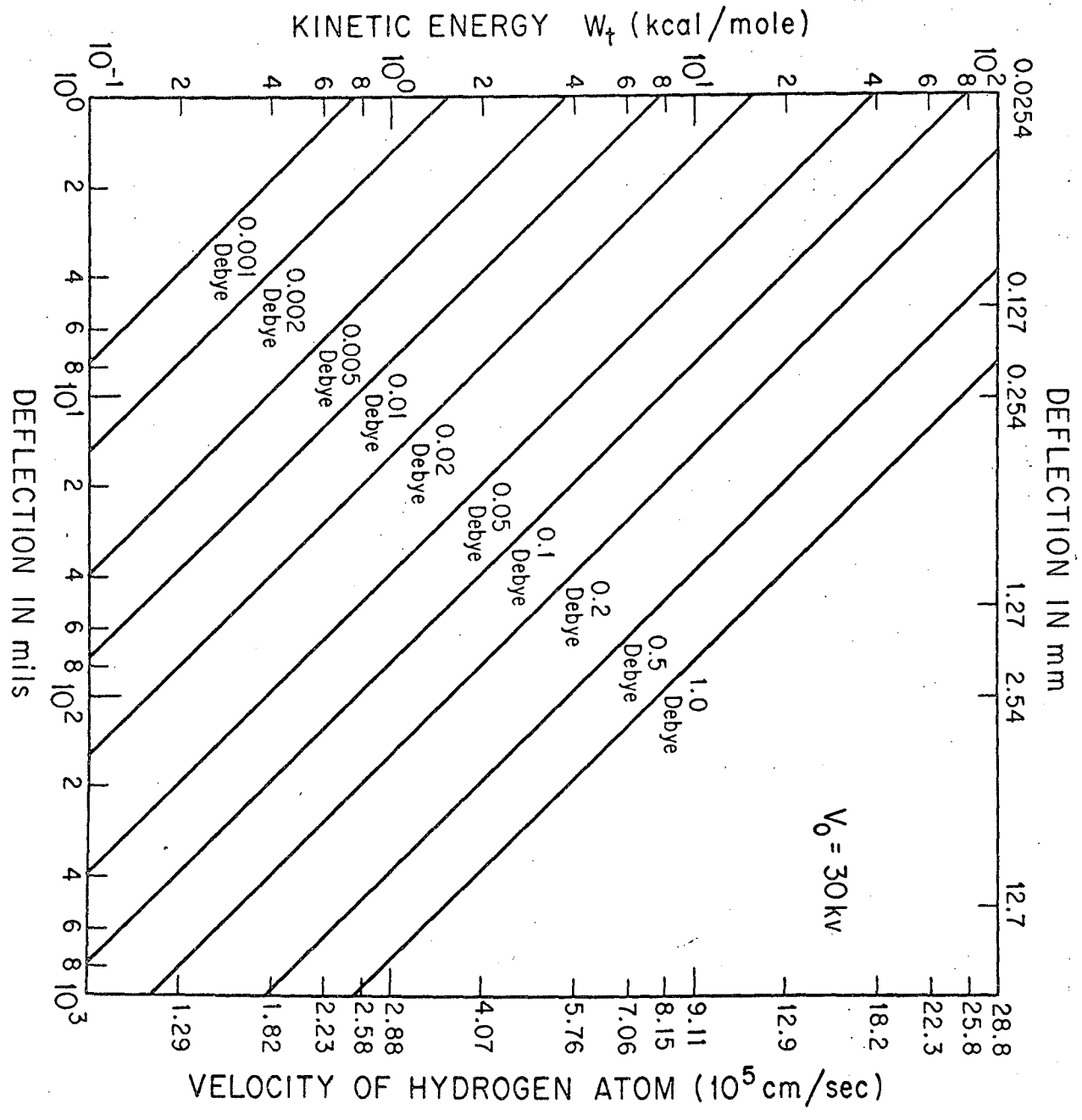

Fig. 2. Deflecting power of field at thirty kilovolts. The deflection curves refer to various values of the effective dipole component in the direction of the electric field.

readily be used to estimate the size of the deflection for any value of the applied potential, since the deflection will depend only on the product of μV_o or $\mu_e V_o$ respectively.

DESCRIPTION OF APPARATUS

A schematic of the molecular beam apparatus, as viewed from above, is shown in Fig. 3 and important dimensions (not shown in Fig. 3) are listed in Table I. Norris[16] and Wilson[17] have described the apparatus in detail, as it is used without the electric field in conventional experiments to measure angular distributions of elastic and reactive scattering.

The two ovens and their cold shields are mounted on a lid which can be rotated about an axis perpendicular to the plane of Fig. 3. Under operating conditions the laboratory angle, Ⓗ, at which scattering events can be observed by the detector may be varied from -30° to +120° (by convention, the sign of Ⓗ as depicted in Fig. 3 is positive). Rotation beyond these limits is prevented by contact between the field collimation system and an oven cold shield.

In order to study the distribution in the direction of the product MX rotation axis, $p(M_J')$, the field housing was designed such that the field, the field collimation slits S_1 and S_2, and the detector could be rotated as a unit while maintaining a vacuum. The axis of rotation of the field is indicated in Fig. 3; rotations of the field about this axis will be indicated by the angle ψ. The field direction shown in Fig. 3 is defined as the normal direction ($\psi = 0°$); by rotating the housing

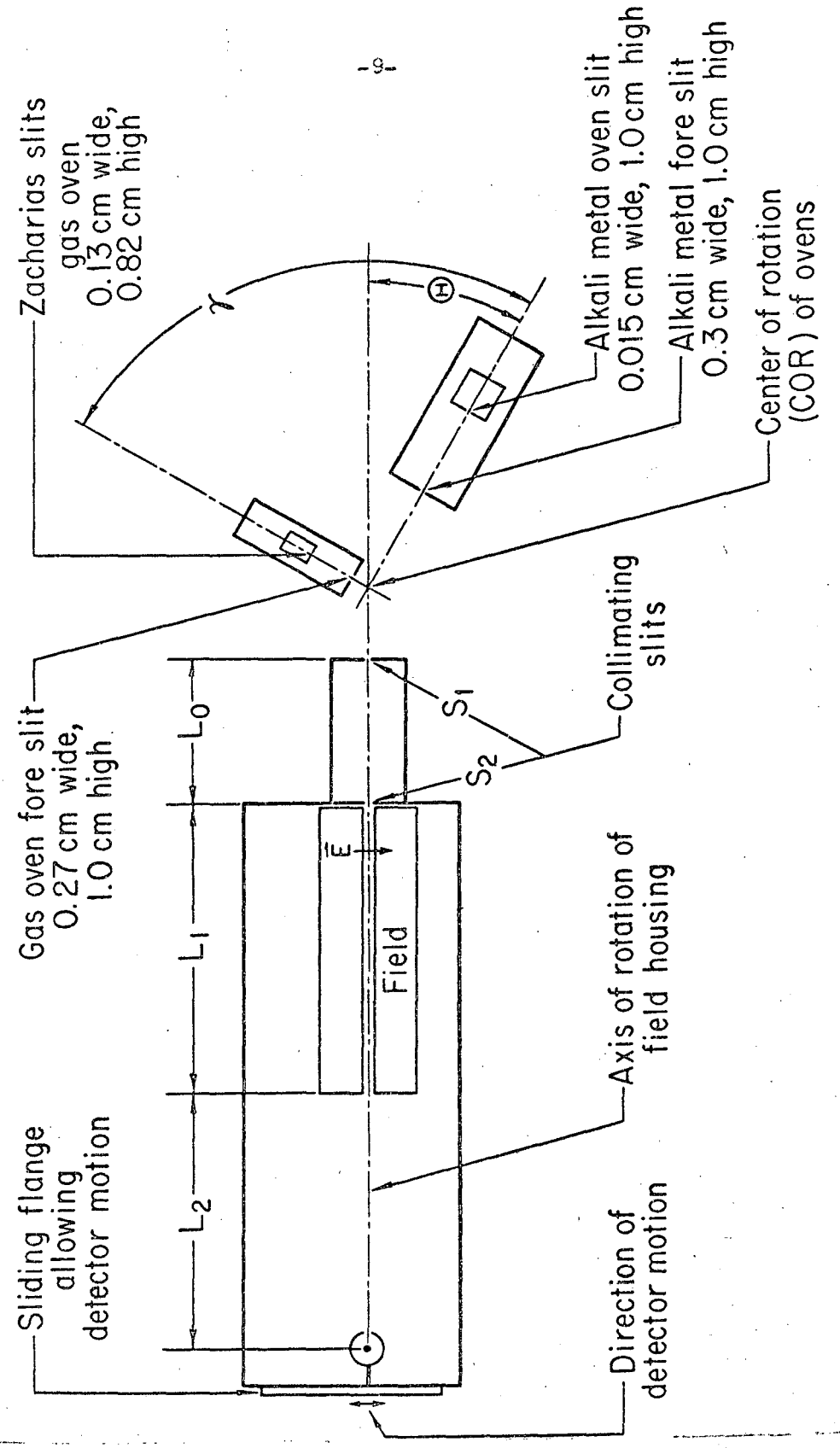

Fig. 3. Schematic diagram of apparatus. The two ovens and their cold shields are mounted on a lid which may be rotated about the scattering center; the field is mounted on a side wall of the vacuum chamber and may also be rotated.

Table I. Apparatus dimensions.[a]

Description	Symbol	Where Defined	Magnitude inches	Magnitude cm
		Alkali Oven		
Distance COR to oven slit		Fig. 3	4.2	10.7
Distance COR to collimating slit		Fig. 3	2.2	5.7
		Gas Oven		
Distance COR to oven slit		Fig. 3	1.3	3.4
Distance COR to collimating slit		Fig. 3	0.35	0.9
		Electrode Dimensions		
Radius - convex electrode (β = 0.785)	a	Fig. 6	0.125	0.318
Radius - concave tip (γ = 1.108)		Fig. 6	0.155	0.396
Spacing parameter	b	Fig. 6	0.125	0.318
Spacing parameter	c	Fig. 6	0.250	0.635
Length	L_1	Fig. 3	6.00	15.24
		Field Assembly		
Height of S_1	H_1	Fig. 3	0.25	0.635
Height of S_2	H_2	Fig. 3	0.25	0.635
Width of S_1	S_1	Fig. 3	0.004	0.010
Width of S_2	S_2	Fig. 3	0.004	0.010
Distance COR to S_1		Fig. 3	1.5	3.9
Distance S_1 to S_2	L_0	Fig. 3	3.00	7.62
Distance front of field to S_2		Fig. 3	0.625	1.6

Description	Symbol	Where Defined	Magnitude inches	Magnitude cm
Length of field	L_1	Fig. 3	6.00	15.24
Distance rear of field to detector	L_2	Fig. 3	5.10	12.97
Height of detector wire		Fig. 3	0.250	0.635
Diameter of detector wire	w_D	Fig. 3	0.003	0.0076
Half width of beam penumbra	p	Eq. 13a	0.002	0.0051
Half width of beam umbra	d	Eq. 13b	0.017	0.0427

[a]COR denotes the center of rotation of the lid on which the two ovens are mounted; for ideal alignment this is the center of the scattering zone.

from behind the detector mount, the field direction may be rotated by as much as 180° in a counter-clockwise sense, corresponding to a change in ψ of +180°. Thus the direction of the field may be varied with respect to the plane defined by the reactant beams and containing the relative velocity vector of approach. For ψ = 0° or 180°, the field direction lies in this plane while for ψ = 90° it is orthogonal to it.

The "Two-Wire" Field

The electrodes were designed to conform to two members of the family of equipotential cylinders of the field conjugate to that produced by two infinitely long parallel conductors of infinitesimal diameter poses-sing equal but opposite charge density and separated by a distance of 2a. The field configuration is shown in Fig. 4. This "two-wire" field has been used in most molecular beam experiments that employ an inhomo-geneous diverging field, including the first electric resonance experi-ment by Hughes.[18] The electrodes and the corresponding field configura-tion are also congruent to those used to produce the standard "two-wire" magnetic field, introduced by Rabi, Kellogg, and Zacharias[19-21]. The dimensions and construction details for the field described here closely parallel those described by Hebert.[22]

The potential at any point between the electrodes may be shown to be[22]

$$V(y,z) = V_o\{\gamma - 1/2(\delta_2-\delta_1)\}/(\gamma-\beta) \qquad (5)$$

where

$$\gamma = \tan^{-1} c/a, \qquad (6a)$$

$$\beta = \tan^{-1} b/a, \qquad (6b)$$

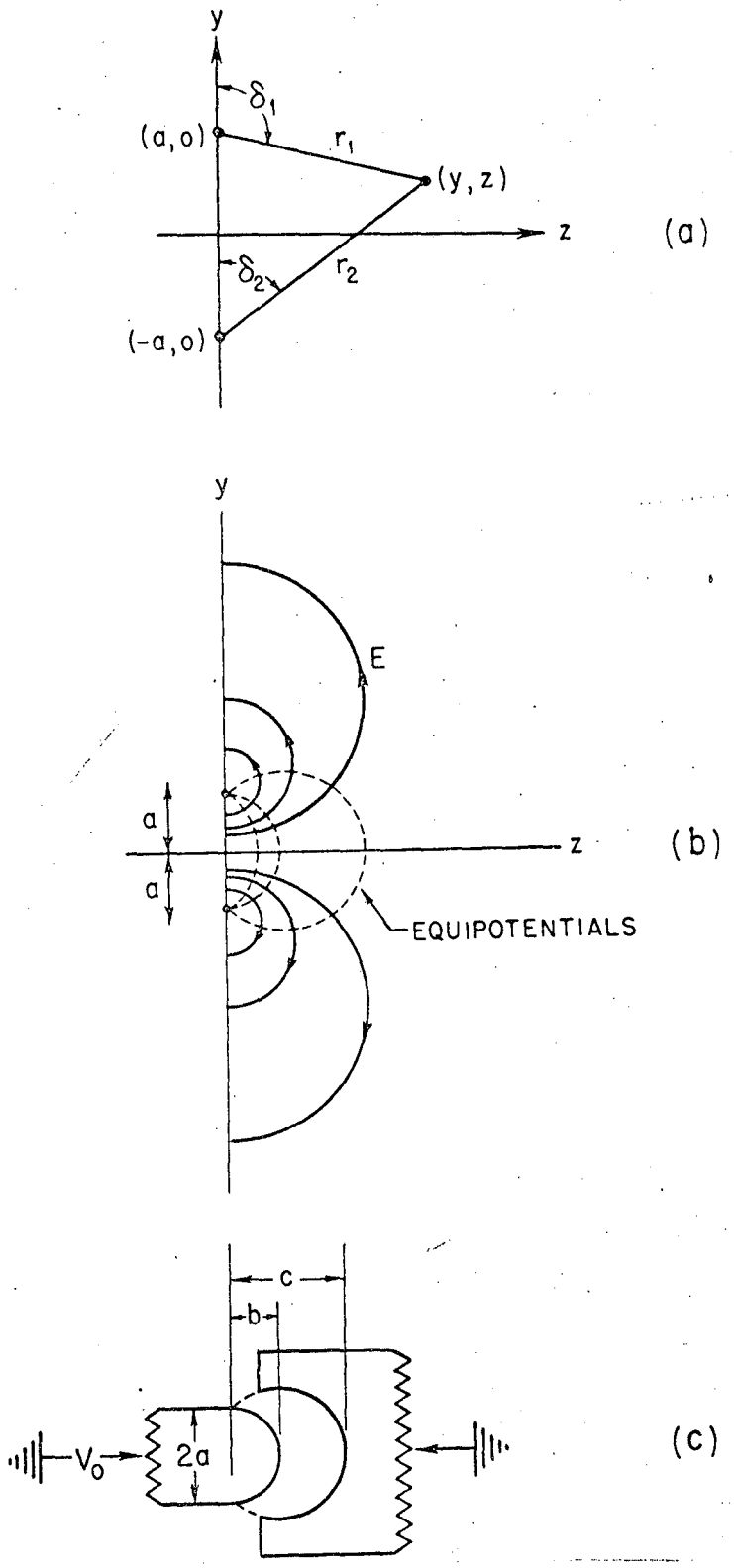

Fig. 4. The "two-wire" field: (a) Coordinate system. (b) Electric field lines (solid curves) and equipotentials (dashed curves) of the field conjugate to that produced by two ideal wires separated by a distance of 2a. (c) Schematic of actual electrode construction and assembly.

and the other parameters are defined in Fig. 4. By differentiating Eq. (5), the following expressions for the field and its gradient are obtained:

$$E_z = \frac{V_o}{2(\gamma-\beta)}\left(\frac{y+a}{r_2^2} - \frac{y-a}{r_1^2}\right),$$

$$E_y = -\frac{V_o}{2(\gamma-\beta)}\left(\frac{z}{r_2^2} - \frac{z}{r_1^2}\right),$$

$$E = \sqrt{E_z^2 + E_y^2} = \frac{V_o}{\gamma-\beta}\frac{a}{r_1 r_2}, \text{ and} \tag{7}$$

$$\frac{\partial E}{\partial z} = -\frac{V_o a}{\gamma-\beta}\frac{z(r_1^2 + r_2^2)}{r_1^3 r_2^3}. \tag{8}$$

The beams which traverse the field are narrow, but about 0.6 cm tall, implying that $-1.0 \lesssim y/a \lesssim 1.0$. Thus, any force in the y direction is of no concern as the y-deflections suffered by a particle are much smaller than the height of the beam. However, the force in the z direction must be as strong as possible and must show little dependence on the y coordinate at a given z.

Since the Stark effect for the interaction of either atoms or polar diatomic molecules in a $^1\Sigma$ electronic state will be second order in E, the z component of the force experienced by such particles will be proportional to $E\partial E/\partial z$. The variation in this function with z is shown in Fig. 5(b); the force on the dipole and therefore the deflection it suffers is seen to be a strong function of its position in the field. However, the criterion that the z component of the force exhibit slight dependence on y is well satisfied, as indicated in Fig. 5(a). This weak dependence of F_z on y holds for all values of z within the field gap.

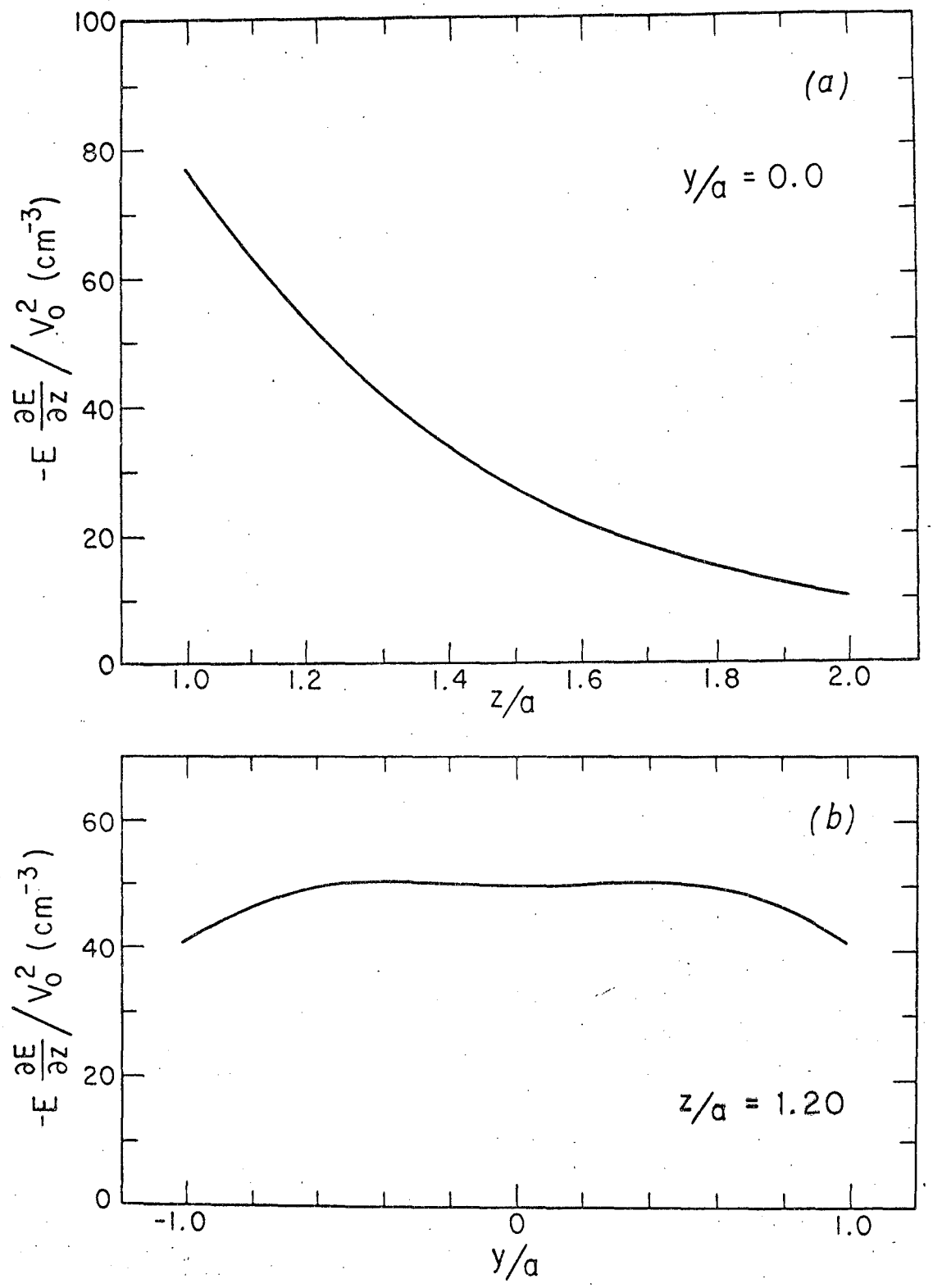

Fig. 5. Plot of the force arising from a second order Stark effect as a function of position within the field. The reduced product of the field and gradient, which is plotted as the ordinate, is independent of V_o.

Details of Construction

A detailed drawing of the electrodes is shown in Fig. 6, where all dimensions are quoted in inches. The field between the electrodes is produced by applying a positive potential, V_o, to the convex electrode and grounding the concave electrode. The electrodes were machined from stainless steel, and the final smooth surfaces were achieved by grinding in order to minimize problems from sparking. In spite of this, sparking proved to be a problem. Thus, during a typical experiment, the applied potential was initially limited to below 10 kv. However, by slowly increasing the potential, the sparking appeared to clean the surfaces, so that after about an hour, it was possible to apply up to 25 to 30 kv before sparking would occur.

Two photographs of the assembled field are shown in Fig. 7, and an assembly drawing of the field is shown in Fig. 8. The entire field, which is 6 inches in length, is mounted in a brass cylinder. The convex pole piece is insulated from the grounded tip by four quartz rods, labeled (4), and is clamped in position by applying pressure on two quartz disks, labeled (5). Part (6) is simply a metal skeleton for clamping the convex piece in position. The assembled field can be positioned within the cylinder by means of two sets of clamps; one of these is labeled (7) in Fig. 8. Thus, the field may be moved until some desired position within the field gap, designated ($y = 0$, z), coincides with the center of the housing cylinder.

As mentioned previously, the field and its housing cylinder may be rotated about an axis perpendicular to the plane of Fig. 8. As the field is rotated, the fan attached to the convex electrode maintains

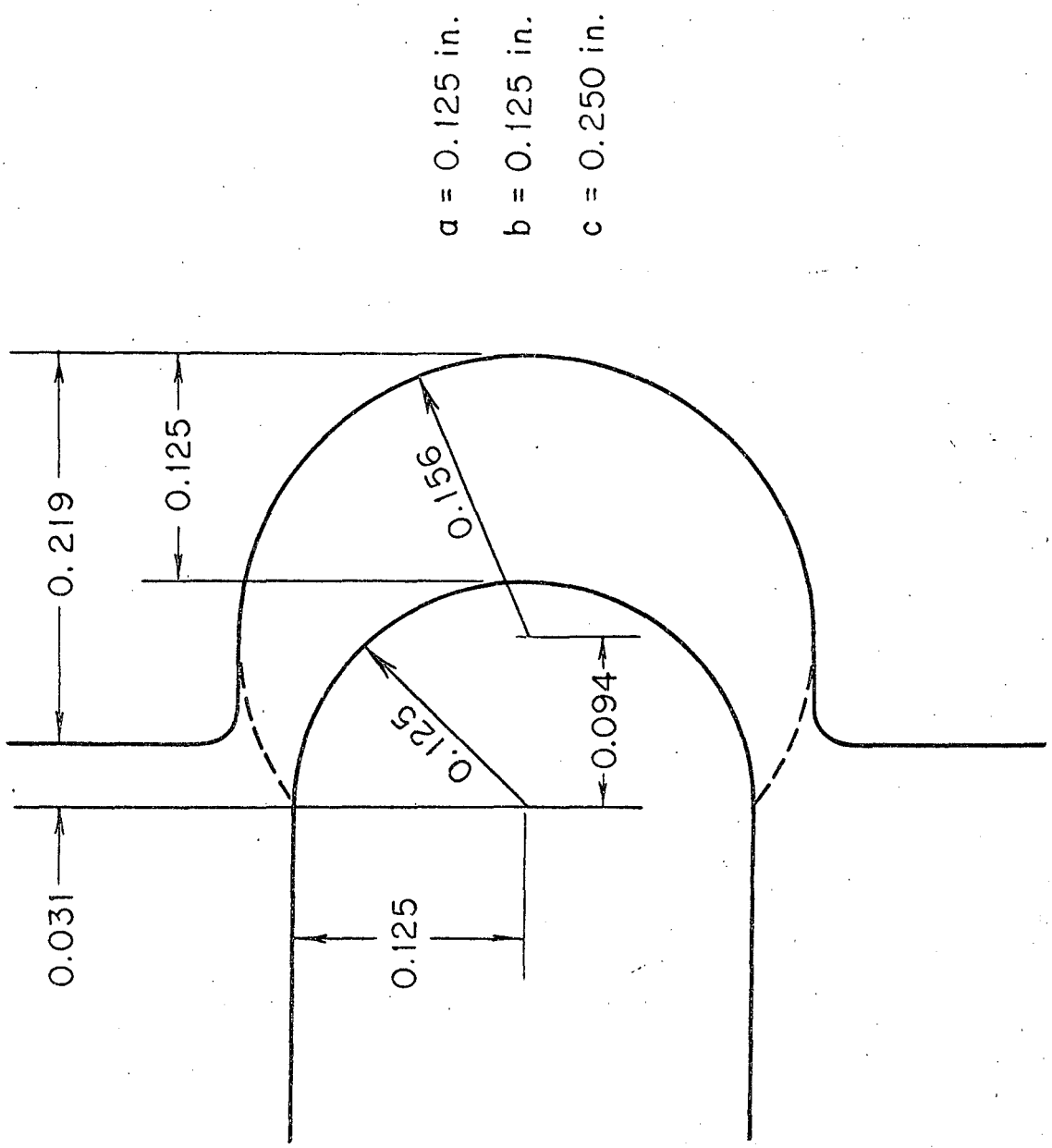

Fig. 6. Details of electrode assembly. All dimensions given in inches.

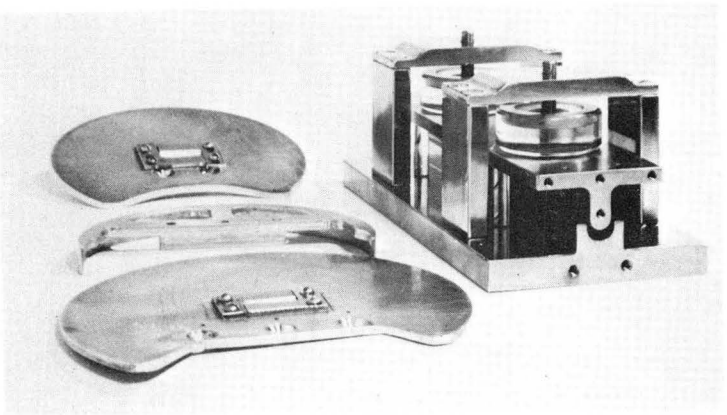

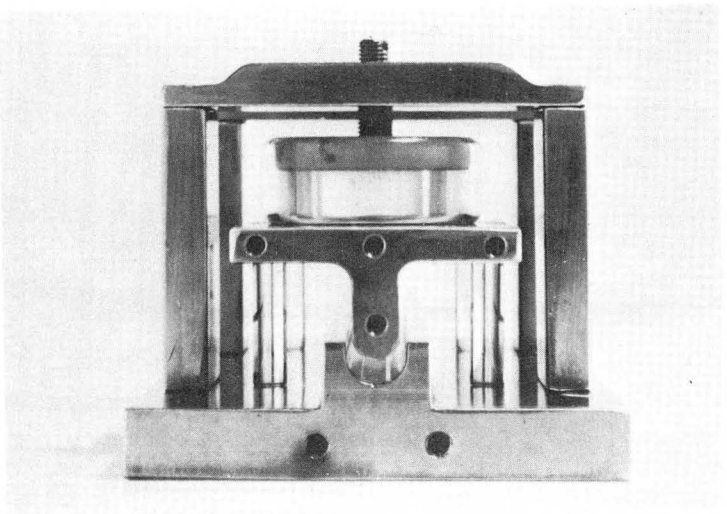

ZN-5084

Fig. 7. Deflecting-field assembly.

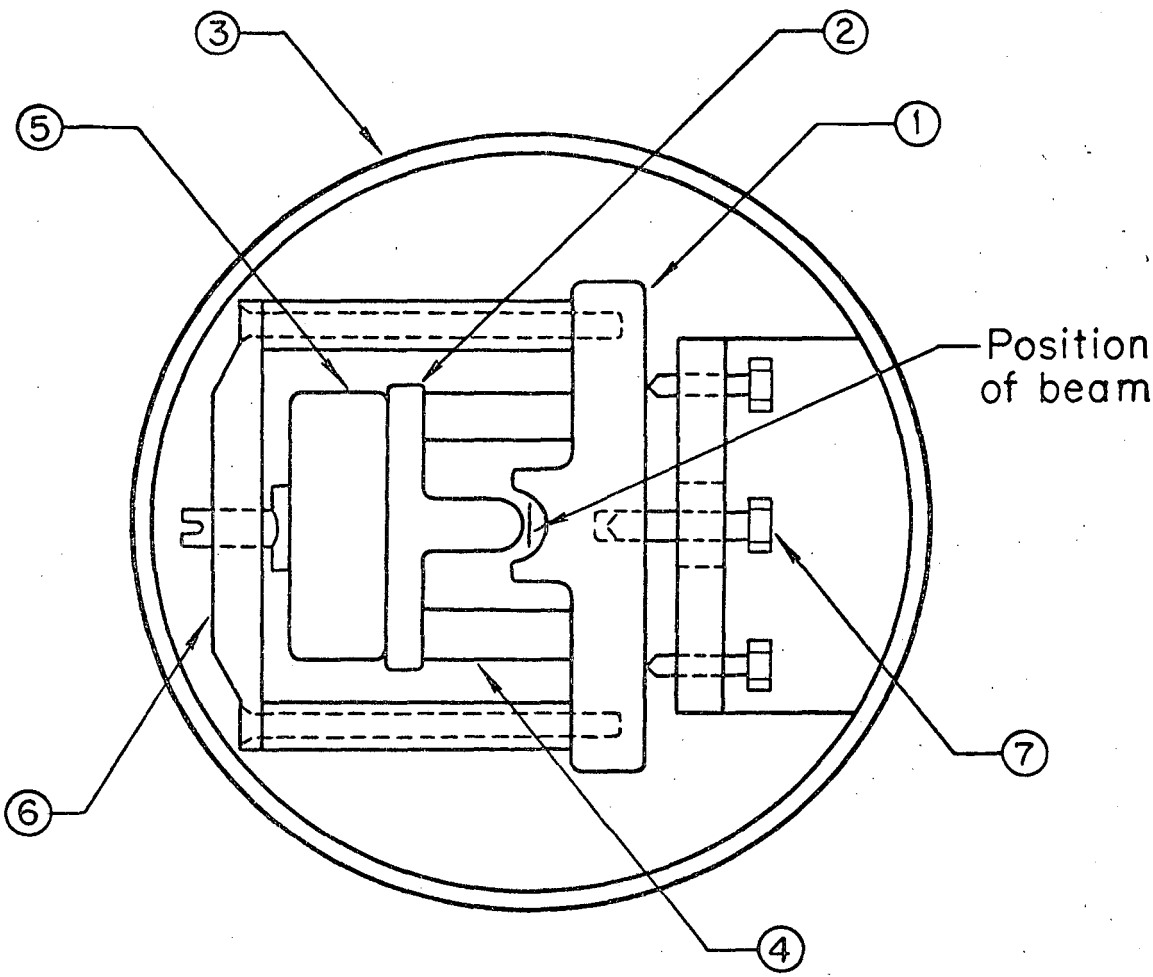

Fig. 8. Assembly drawing of electrodes.

electrical contact with a spring loaded rod as shown in Fig. 9. Thus, a potential is applied to the convex tip through this spring loaded contact for any angle of rotation of the field.

An assembly drawing of the field in its housing cylinder as viewed from the side is shown in Fig. 10 as an integral part of the apparatus ($\psi = 90°$ in this view). A rotating vacuum seal between the cylinder housing and the flange on which it is mounted is indicated in Fig. 10, allowing rotation of the field under vacuum by as much as ±90°. The detector mount is not shown in Fig. 10. A Langmuir surface ionization detector is employed using either a tungsten or an 8% tungsten-92% platinum alloy wire, 0.0076 cm in diameter. The former will ionize an alkali metal or its halide while the latter, when properly treated with methane, ionizes only the alkali metals.[23] The detector is mounted such that it may be moved across the gap of the field while maintaining vacuum; additionally, either detector wire may be rotated during the experiment, without rotating the field housing cylinder, in order to be made to coincide with the plane of the beam traversing the field. Also not shown in Fig. 10 are two sheets of gold gauge (80% transmission) between the electric field and the detector; both sheets are grounded to the cylinder housing and are intended to shield the detector from the field. The collimation system in front of the field shown in Fig. 3 is described in a later section.

The field is charged by a power supply capable of supplying up to 50 kilovolts D.C. at a maximum current of 5 milliamperes with less than 2% ripple.[24] The power supply was installed in a well interlocked rack as shown on UCRL Drawing No. 4X7765B/

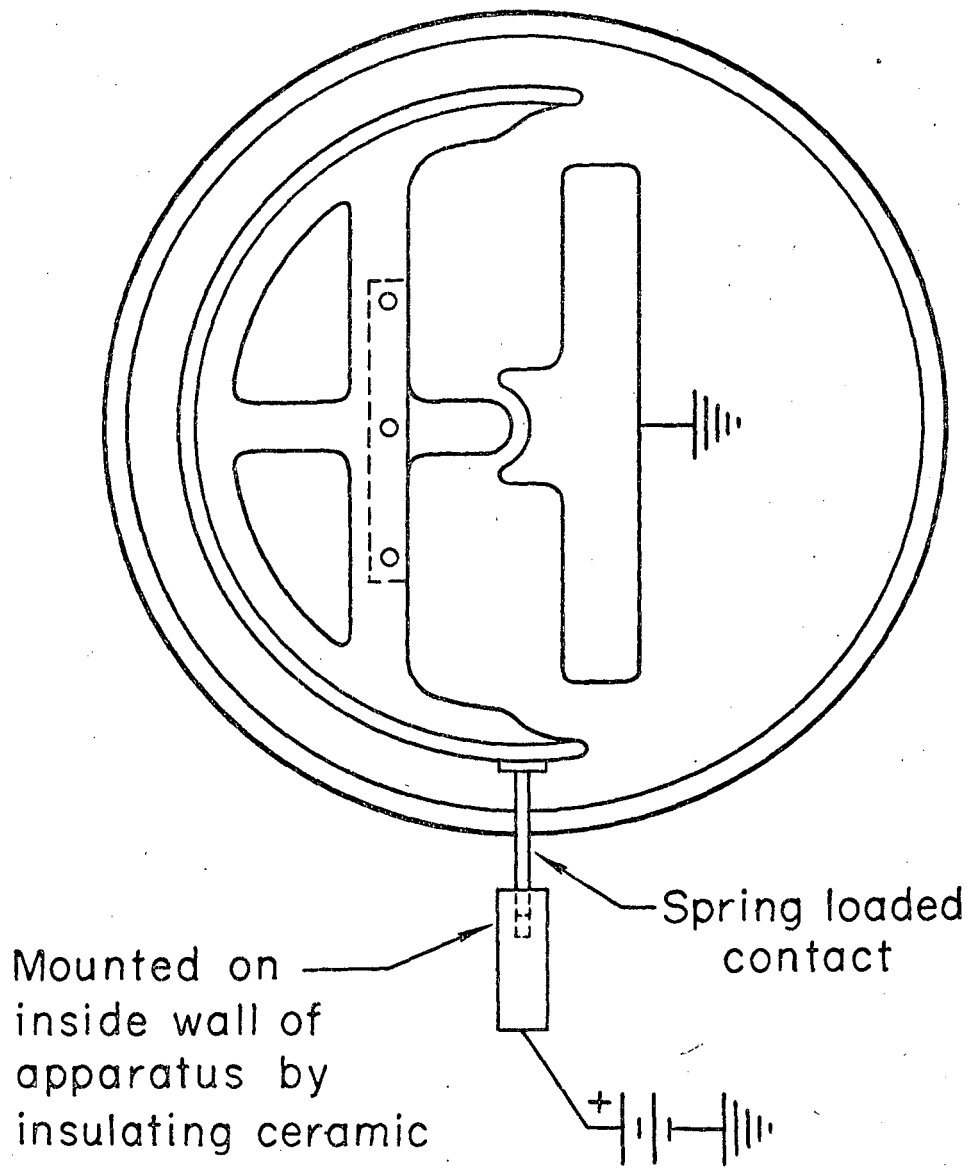

Fig. 9. Schematic drawing showing the method of applying potential to the convex electrode.

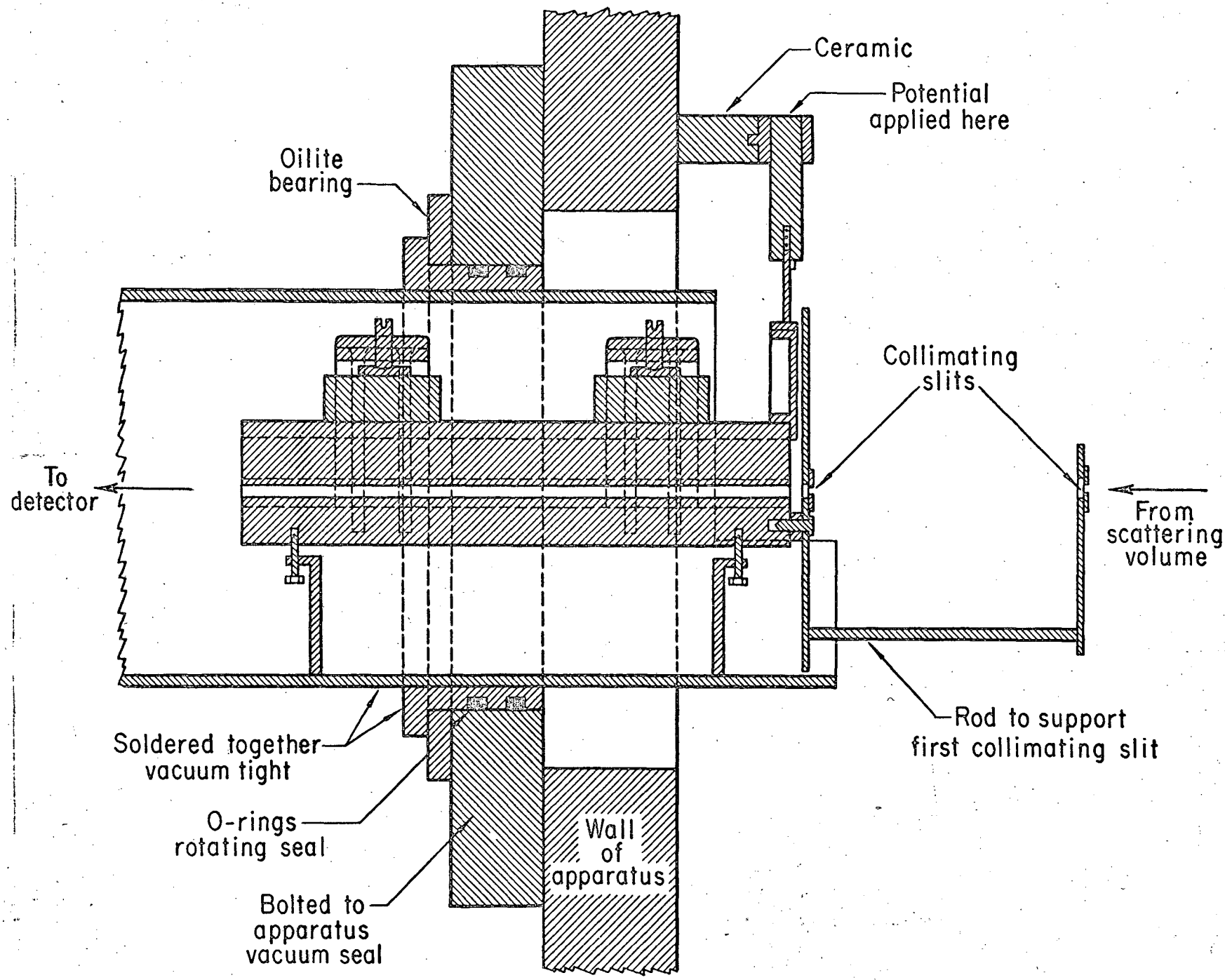

Fig. 10. Assembly drawing of field as it is mounted on the apparatus.

Pumping and Shielding

The apparatus is pumped by two six inch oil diffusion pumps situated on the main chamber which houses the two ovens. The chamber housing the electric field, 10 cm in diameter and 30 cm long, is pumped through the main chamber. In addition, the apparatus exhibits a much higher pumping speed toward condensible gases by virtue of a copper surface lining the inside of the apparatus which is maintained at liquid nitrogen temperature. This cold trapping does not extend into the field housing cylinder. However, the volume between the field collimating slits S_1 and S_2 and the entrance to the field is shielded in such a way that particles scattered out of the beam intersection volume can reach the detector only if they are transmitted through S_1 and S_2.

The uncorrected pressure measured on an ionization gauge in the main chamber during scattering experiments was usually less than about 5×10^{-7} mm Hg. While the pressure in the field housing chamber may have been slightly higher than that recorded in the main chamber, it was certainly sufficiently low to warrant ignoring the effect of scattering of the beam by background gas. Thus the observed shape of the beam in the absence of an applied potential was always close to the theoretical trapezoidal shape predicted for transmissions through the field collimation system (see Figs. 11 and 14 for examples).

EXPERIMENTAL CONDITIONS

The apparatus was constructed such that the rotation in product MX could be investigated in three different ways. The simplest consists

in observing the transmission of MX through the field at an applied potential V_o, that is in observing the attenuation of the MX as a result of the field with the detector positioned at the center of the undeflected beam profile. The observed transmission will allow one to infer some average value of the rotation in the MX, and possibly also some information concerning the rotational distribution function from the functional dependence of the transmission on the applied potential. Alternatively, by measuring the deflection of the beam by the field, it may be possible to invert the observed deflection pattern to obtain the distribution in effective dipole moments within the beam. Finally, by varying the angle of the field, ψ, it may be possible to convert the distributions in effective dipole moments observed at different field angles ψ into the distribution in rotational states, $\rho(J',M_J')$. This distribution in M_J' which is measured with respect to the direction of the field may finally be transformed into the distribution in directions of J' with respect to the relative velocity of approach of the reactants, which is the information to be compared with any theoretical predictions.

Alignment

A successful measurement of the product rotation is critically dependent on the alignment of the apparatus. Both beams and the line of sight through the two field collimating slits must pass through the center of rotation of the lid supporting the ovens (henceforth referred to as the COR); small deviations of any one of these three from this condition may result in a drastic reduction of the experimentally realizable signal. Furthermore, the deflection patterns produced by the

field are a function of the shape of the undeflected beam profile, which is determined by S_1, S_2, L_0, L_1, and L_2 of Fig. 3; consequently, all of these parameters must be reproduced on each experiment. In addition, the position of the beam in the field must be held constant, as Fig. 5(b) illustrated the strong dependence of the force on the z coordinate. The three lines of sight were aligned to intersect at the COR by the procedure described below. To insure identical geometry within the field region during different experiments, neither the field nor either of its collimating slits were removed when the apparatus was opened and altered (usually by way of recharging the alkali oven) subsequent to the primary alignment.

Primary Alignment Procedure

The center of rotation (COR) of the lid is determined by suspending a weighted thread from the lid and varying its position until it is found to remain stationary upon rotating the lid. As the axis of rotation of the field housing was designed to intersect the axis of rotation of the lid, a cathetometer is positioned looking down the axis of the field housing and through the COR.

With the field in its normal direction ($\psi = 0°$) it is then positioned within its housing such that the cathetometer line of sight is parallel to the equipotentials and at approximately $y = 0$, $z = 1.2a$; the two oven and cold shield slits are subsequently aligned along the cathetometer sighting. The detector and the field collimating slits S_2 and S_1 are then aligned in that order along the cathetometer line of sight. The most critical requirement in the optical alignment is that the field slit system S_1 and S_2 be looking through the COR. Optical

alignment of the detector is unimportant, as it can be positioned accurately during the experiment by maximizing the signal recorded for the undeflected beam.

Beam Conditions

In addition to thermal distributions in velocity, both beams are formed with considerable angular spread due to the poor beam collimation imposed by intensity limitations. Employing electron bombardment ionization and a four-pole mass spectrometer, Wilson[17] found that the gas beam has a full width at half intensity of $\sim 12^\circ$ and that the beam shape was roughly triangular. While the alkali atom beam profile differed from those previously reported, it was not measured during these experiments, as such a measurement would have necessitated removing the field collimating slits. From the widths and positions of the alkali oven and cold shield slits, a roughly square profile with a spread of $\sim 3.5^\circ$ is expected. These angular spreads imply a scattering volume defined by a beam of alkali atoms ~ 0.6 cm wide and of constant intensity crossed at an angle γ, which will usually be 90°, by a gas beam with a triangular beam intensity and a full width at half maximum of about 0.65 cm.

As the scattering volume is not cylindrically symmetric, a correction would have to be applied to angular distributions measured on the present detector, which sees only a fraction of the total scattering volume. This arises as the effective volume in the case of detector collimation may be a function of the angle of observation, Θ. In fact, however, the only information obtained from conventional angular distribution measurements, where the detector can see the entire scattering

volume, which is necessary for this experiment will be the percentage of the signal recorded at a given angle which arises from nonreactive scattering of atoms. This number will not be affected by the detector collimation. Knowledge of the percentage atoms scattered is necessary to interpreting this experiment in that the observed deflection patterns will be composed of those resulting from both atomic and molecular deflections.

Estimate of Expected Signal

The ratio of accessible signal in this experiment to that obtained in a conventional experiment, where the detector views the entire scattering volume, is $SH_p/0.6H$ where $S = S_1$, H_p is the height of S, and H is the normal height of the scattering volume. Employing the experimental dimensions cited earlier, this number is approximately $(.01)(.65)/.6x1 \sim 1\%$. In addition, an intensity factor of roughly five is lost as the detector is further away from the collision zone than in conventional experiments. Thus, the scattered signals detected in this experiment should be about five hundred times weaker than those observed in conventional experiments where one simply measures the scattered signal versus laboratory angle. Unfortunately, this intensity problem cannot be improved much by widening the slits or shortening the distance from scattering zone to detector. As the angular momentum of product MX is to be determined by observing the MX deflection upon traversing the field, the width of the undeflected beam must be comparable to or smaller than the molecular deflections, thereby limiting S_1 to the neighborhood of the experimental value chosen. For the same reason,

the length of the field cannot be shortened, as the molecular deflection is proportional to the square of this length.

The signal levels reported[7] in the study of product rotational excitation in the reaction of potassium with bromine are typical of the signals which are experimentally realizable. The potassium oven temperatures were 613°K and 651°K for the lower and upper chambers respectively. The bromine was prepared on a glass vacuum line outside of the main chamber at a pressure of ~250 μ (as measured on a Hastings thermocouple gauge) and effused from the gas oven at a temperature of 316°K. This resulted in a peak K beam signal transmitted through the collimating slits of $\sim 10^{-8}$ amperes which was attenuated ~40% by the crossed Br_2 beam. The peak scattered signal recorded at $\Theta = 30°$ was $\sim 2 \times 10^{-13}$ amperes, or 0.002% of the potassium beam signal.

Distortion of Polarization

There are four effects which may tend to distort the measurement of the M_J' distribution of product MX by observing its deflection in the field. Once the MX is formed in a reactive collision and is in transit to the field, it is isolated in space. Then there will be a weak coupling of $\underset{\sim}{J}'$ to the nuclear spins of M and X. This coupling should not alter the value of J', but it may introduce an uncertainty in M_J', as later measured by the field, of the magnitude of the total nuclear spin. Experimentally, this distortion of the M_J' distribution could be prevented by imposing a homogeneous field across the region between the collision volume and the inhomogeneous field; this would serve to couple M_J' strongly to the field direction as long as the interaction with the field were stronger than the intramolecular

hyperfine interactions. In fact, however, even in the most favorable case, the distribution in M_J' resulting from reaction will be expected to exhibit a spread in M_J' comparable to or greater than the distortions which can be introduced by the nuclear spins. Thus, the effect of nuclear spins, even in the absence of a field imposed across the reaction zone, should be confined to a slight broadening of the M_J' distribution.

The information of interest for comparison with any theoretical predictions is an experimental determination of the distribution in the projections of $\underset{\sim}{J}'$ onto the relative velocity with which the reactants approach. However, the thermal distributions in velocities of the two crossed beams will result in a distribution in directions of this relative velocity, implying a broadening of the M_J' distribution which may be measured. This effect does not then distort the measured laboratory distribution in directions of J' with respect to the electric field direction; rather, it obscures the information concerning the direction of J' in the coordinate system appropriate to the reaction which may be deduced from the measured laboratory distribution. Velocity selection of one or both reactant beams would reduce this spreading, but of course such selection reduces the attainable intensity. This distortion of the M_J' distribution may be calculated, as it is possible to calculate the distribution in directions of the relative velocity of the reactants.[25]

The slight variation in $E\partial E/\partial z$ with y was shown in Fig. 5(a). However, this does not imply such a small variation in F_z, insofar as the direction of the field varies appreciably with y; thus, at $z = 1.2a$,

the angle the field makes with the line y = 0 varies from ~60° to ~-60° as y varies from a to -a. Consequently, if the MX products enter the field without distortion in the rotation axis direction, the value of M_J' seen by the field will vary appreciably over the height of the beam. This effect will soon be corrected by the addition of electrodes (not described in this report) attached to the front of the field electrodes, which will be designed such that the entering MX first sees a uniform electric field. This buffer field will be designed to merge continuously from a uniform field directly behind the second collimating slit S_2 into the "congruent two-wire" field slowly enough that the M_J' states of the alkali halide should adiabatically follow the change in field direction. Experimentally, these buffer fields can be designed as an extension of the two pole faces already discussed; their surfaces will then be cut off at an angle such that at one end they merge into the existing electrodes, while at their front end they merge into two plane parallel electrodes.

A fourth origin of distortion of the M_J' distribution which can be induced by the present experimental design arises from the possibility of transitions between M_J' states as they are entering the field. The magnitude of this effect is enhanced by high field strength and by a rapid build-up of the field. Experimentally, the buffer field described above should also result in appreciable reduction of the field strength at the entrance to the field, thereby inhibiting this effect. Further, by replacing the metallic collimating slit S_2 by one constructed of an insulator, the fringing field originating at the end of the buffer electrodes should extend through S_2, thereby securing a less abrupt rise in the field strength.

THEORY OF DEFLECTION PATTERNS

Theoretical expressions characterizing the deflections of beams of atoms or polar molecules are developed in this section. Tables IIa and IIb summarize a number of useful relations, in terms of the physical parameters and as working formulae respectively.

Calculation of Effective Dipole Moments

Any atom or molecule will interact with an external field due to the distortion of its field free charge distribution by the field. The induced dipole moment in the case of alkali atoms will be given to first order by

$$\mu_p = \alpha E, \tag{9}$$

where α is the scalar atomic polarizability. The resulting induced force,

$$F_z = \alpha E \frac{\partial E}{\partial z},$$

will always accelerate the alkali atoms towards the high field region; in this report deflections toward the high field region are taken as positive by convention.

The deflection of a beam of alkali halides is far more complex than that of an alkali metal beam. In addition to a thermal distribution in velocities and the intensity distribution at zero field, it is necessary to consider distributions in M_J and J states, as the effective dipole and therefore the force will be different for different rotational states.

Table IIa. Summary of relations

Quantity	Symbol	Relation
Field	E	$aV_o/r_1r_2(\gamma-\beta)$
Field gradient	$\partial E/\partial z$	$-aV_o z(r_1^2+r_2^2)/r_1^3r_2^3(\gamma-\beta)$
Moment of inertia	I	$m_1m_2r_m^2/(m_1+m_2)$
Rotational constant	B	$h/8\pi^2cI$
Induced moment polarizability	μ_p	αE
Rotational energy	W_r	$hcBJ(J+1)$
Translational energy	W_t	$1/2mv^2$
Electrical energy	W_e	$-\int_0^E \underset{\sim}{\mu}_i \cdot d\underset{\sim}{E}$
Effective moment rotating dipole	μ_e	$\mu f(E)G(J,M)$, $f(E) = -\frac{\mu E}{W_r}$ $G(J,M) = \frac{J(J+1)-3M^2}{(2J-1)(2J+3)}$
Force on induced moment	F_z	$\mu_e \partial E/\partial z$
Deflection	s	$FL_1(L_1+2L_2)/2mv^2$
	s_α	$F_z L_1(L_1+2L_2)/4kT_t$
	s_α^o	$\mu^2 E\partial E/\partial z L_1(L_1+2L_2)/8k^2T_tT_r$

Table IIb. Useful working formulae

Quantity	Symbol	Unit	Working formula
Potential	V_o	volt	
Apparatus dimensions		cm	
Bond lengths	r_m	$\mathring{A}$	
Mass	m	gms/mole	
Polarizability	α	$\mathring{A}^3$	
Temperature	T	°K	
Velocity	v	10^4 cm/sec	
Dipole moment	μ	Debye	
Field	E	volt/cm	$0.9921\frac{V_o}{r_1 r_2}$
Field gradient	$\frac{\partial E}{\partial z}$	volt/cm^2	$-0.9921\frac{z(r_1^2+r_2^2)V_o}{r_1^3 r_2^3}$
Moment of inertia	I	$\frac{gm\text{-}\mathring{A}^2}{atom}$	$1.659\times10^{-24}\frac{m_a m_b}{m_a+m_b} r_m^2$
Rotational constant	B	cm^{-1}	$2.7987\times10^{-23}/I$
		megacycles	$8.3902\times10^{-19}/I$
Induced moment polarizability	μ_p	Debye	$3.3356\times10^{-9}\alpha E$
Rotational energy	W_r	kcal/mole	$2.860\times10^{-3}BJ(J+1)$
Translational energy	W_t	kcal/mole	$1.195\times10^{-3}mv^2$
Electrical energy	W_e	kcal/mole	$-4.8032\times10^{-8}\int_0^E \underset{\sim}{\mu_i}\cdot d\underset{\sim}{E}$
Induced moment rotating dipole	μ_e	Debye	$-1.6794\times10^{-5}\frac{\mu^2 EG(J,M)}{BJ(J+1)}$
Force on induced moment	F	dynes	$3.3356\times10^{-21}\mu_e\cdot\frac{\partial E}{\partial z}$

Table IIb. (continued)

Quantity	Symbol	Unit	Working formula
Deflection	s	cm	$1.005\times10^{-5}\ \dfrac{\mu_e \circ \frac{\partial E}{\partial z} L_1 (L_1+2L_2)}{mv^2}$
	s_α	cm	$6.042\times10^{-6}\ \dfrac{\mu_e \circ \frac{\partial E}{\partial z} L_1 (L_1+2L_2)}{T_t}$
	s_α^o	cm	$7.301\times10^{-11}\ \dfrac{\mu^2 E \circ \frac{\partial E}{\partial z} L_1 (L_1+2L_2)}{T_t T_r}$

The perturbation term in the Hamiltonian for the interaction of a permanent dipole moment with an external electric field E is expressed as

$$H = -\underset{\sim}{\mu} \cdot \underset{\sim}{E};$$

$\underset{\sim}{\mu}$ is the permanent dipole fixed along the internuclear axis of the molecule which is rotating in the laboratory about the total angular momentum $\underset{\sim}{J}$. An alkali halide in its $^1\Sigma$ electronic ground state will not experience any Stark perturbation to first order, as the first order time averaged component of the dipole moment in the direction of the field will be zero. Second-order quantum mechanical perturbation theory predicts that the potential energy of the alkali halide in the field will be[1]

$$W^{(2)}_{J,M_J} = \frac{\mu^2 E^2}{hcB} \frac{J(J+1)-3M_J^2}{2J(J+1)(2J-1)(2J+3)} \tag{10}$$

where B is the molecular rotation constant. Eq. (10) is valid in the strong field limit, which will always prevail in these experiments, where the perturbation of the dipole by the field is larger than the intramolecular hyperfine interactions. Differentiating Eq. (10), the effective component of the dipole moment to second order is obtained as:

$$\mu_e(J,M_J) = f(E)G(J,M_J) \tag{11}$$

where

$$f = \frac{-\mu E}{hcBJ(J+1)} = \frac{-\mu E}{W_r}, \tag{11a}$$

$$G(J,M_J) = \frac{J(J+1) - 3M_J^2}{(2J-1)(2J+3)}, \tag{11b}$$

and W_r is the rotational energy. In the classical limit where J is large and

$$M_J/J = \cos\phi,$$

ϕ being the angle between $\underset{\sim}{J}$ and $\underset{\sim}{E}$, Eq. (11) agrees with a second order classical expression due to Stern.[25] Thus the force acting on a polar diatomic in an inhomogeneous electric field will differ for different rotational states and may accelerate the dipole on either high or low field depending on M_J/J.

The perturbation energy given in Eq. (10) will suffice to describe the deflection of thermal energy alkali halide beams. The most important correction terms will arise from the fourth-order Stark effect term and the induced dipole moment due to the polarizabilities of the alkali halides; incorporation of these corrections modifies Eq. (10) to read

$$W_{J,M_J} = W^{(2)}_{J,M_J} + W^{(4)}_{J,M_J} + W^{(\alpha)}_{J,M_J} \qquad (10a)$$

where the polarizability may now be a tensor interaction.

The fourth-order Stark perturbation term has been given by Wharton, Kaufman, and Klemperer as[27]

$$W^{(4)}_{J,M_J} = \frac{\mu^4 E^4}{(hcB)^3} f(J,M_J)$$

where $f(J,M_J) = A + B + C + D$

and:

$$A = \frac{(J^2-M_J^2)((J-1)^2-M_J^2)}{8J^2(2J-3)(2J-1)^3(2J+1)}$$

$$B = \frac{((J+1)^2-M_J^2)(M_J^2-(J+2)^2)}{8(J+1)^2(2J+1)(2J+3)^3(2J+5)}$$

$$C = \frac{(J(J+1) - 3M_J^2)(M_J^2 - (J+1)^2)}{8J(J+1)^3(2J-1)(2J+1)(2J+3)^2}$$

$$D = \frac{(J(J+1) - 3M_J^2)(M_J^2 - J^2)}{8J^3(J+1)(2J-1)^2(2J+1)(2J+3)} .$$

Calculations of the fourth-order interaction for a thermal beam (850°K) of CsCl justify neglecting its contributions. Thus, for the most probable J value in the beam (∿65) and an applied potential of 25 kv, the fourth-order term is always less than 1% of the second-order term. These small perturbations on the second order term can be neglected because they are important only for very low and therefore improbable J states; even for these states, the fourth-order contribution probably won't be important until the applied potential is sufficiently high that the molecules are deflected beyond the range of scan of the detector. In fact, it is probably the fate of these very low J values to hit the electrodes and so not be transmitted through the field.

The matrix elements referring to the polarizability interaction have been evaluated by Marshall and Weber[28] for a linear rotor as

$$W^{(\alpha)}_{J,M_J} = -\frac{1}{2}\alpha_d E^2 F(J,M_J) - \frac{1}{2}\alpha_{xx}E^2$$

where $\alpha_d = \alpha_{zz} - \alpha_{xx}$. As the polarizabilities of all of the alkali halides will be small (see Appendix I), Eq. (11) should be a very good approximation to the effective dipole moment, although the most important correction would be the polarizability interaction.

Effect of Beam Shape and Velocity Distribution

Consider the profile of a beam transmitted through the field collimating slits S_1 and S_2 at zero field. Scattered flux entering S_1 originated in the scattering volume; in the case of thermal beams for calibration, the alkali metal oven was used to form the beam and no crossed gas beam was present. In either case, the source is sufficiently wider than S_1 to be regarded as infinitely broad. Under these conditions, the zero field intensity f versus detector position s_o will be given by[29]

$$f(s_o) = I_o \frac{d+s_o}{d-p}, \quad -d < s_o < -p \tag{12a}$$

$$f(s_o) = I_o, \quad -p < s_o < p \tag{12b}$$

and

$$f(s_o) = I_o \frac{d-s_o}{d-p}, \quad p < s_o < d \tag{12c}$$

where I_o is the flux at the center of the beam. The parameters p and d are defined by

$$p = \tfrac{1}{2}S_2 + (S_2 - S_1)R, \tag{13a}$$

$$d = \tfrac{1}{2}S_2 + (S_2 + S_1)R, \tag{13b}$$

and

$$R = (L_1 + L_2)/L_o. \tag{13c}$$

The dimensions of the apparatus listed in Table I predict that p = 0.005 cm and d = 0.043 cm.

Assuming the z component of the force to be constant over the dimension of the beam, the deflection experienced by an atom with velocity v and mass m which would arrive at the detector position s_o in the absence

of an applied potential is readily derived to be

$$s - s_o = \frac{F_z L_1 (L_1 + 2L_2)}{2mv^2} \tag{14}$$

where F_z is given by Eq. (1). The deflection of particles traveling with the most probable velocity in the source,

$$\alpha = \frac{2kT_t}{m} , \tag{15}$$

is calculated by Eq. (14) to be

$$s_\alpha = (s-s_o)_\alpha = \frac{F_z L_1 (L_1 + 2L_2)}{4kT_t} \tag{14a}$$

where T is the translational temperature in °K.

In general the z component of the force F_z, will be a function of the quantum state of the particles, e.g., for a polar diatomic $F_z = F_z(J,M_J)$. Accordingly, there exist an s_α corresponding to each populated quantum state in the beam, $s_\alpha = s_\alpha^i$. By a slight extension of the derivation given by Ramsey[30] for the case of magnetic deflection, an expression for the signal measured on a detector of infinitesimal width, $I(s,V_o)$, as a function of detector position s may be derived for the deflection of a beam in one quantum state characterized by s_α^i. By averaging over the assumed thermal distribution in flux velocities, and the shape of the zero field beam profile, the following expression is obtained:

$$I(s,V_o) = 0.0, \quad s < -d$$

$$I(s,V_o) = I_d = \frac{s+d}{d-p} e^{-s_\alpha^i/(s+d)} ,$$

$$-d \leq s \leq -p \tag{16a}$$

$$I(s,V_o) = I_d - I_p = I_d - \frac{s+p}{d-p} e^{-s_\alpha^i/(s+p)}, \quad -p \leq s \leq p \tag{16b}$$

$$I(s,V_o) = I_d - I_p - I_{-p} = I_d - I_p - \frac{s-p}{d-p} e^{-s_\alpha^i/(s-p)}, \quad p \leq s \leq d, \tag{16c}$$

$$I(s,V_o) = I_d + I_{-d} - I_p - I_{-p} = I_d - I_p - I_{-p} + \frac{s-d}{d-p} e^{-s_\alpha^i/(s-d)} \quad d \leq s. \tag{16d}$$

As remarked above, Eq. (16) assumed a thermal distribution in velocities and therefore may not be applicable to the deflection of a beam of alkali halides obtained as products of a chemical reaction. In addition, Eq. (16) is an expression for the relative signal, as I_o of Eq.(12) was set equal to unity. Consequently, $I(s,V_o)$ is normalized such that $\int_{-\infty}^{\infty} I(s,V_o)ds = p+d$. Further, Eq. (16) applies only for $s_\alpha^i > 0$. An analogous expression for $s_\alpha^i < 0$ is obtained by reversing the signs of s_α^i and s:

$$I(s,V_o) = 0.0, \quad s \geq d$$

$$I(s,V_o) = -I_{-d}, \quad p \leq s \leq d \tag{17a}$$

$$I(s,V_o) = I_{-p} - I_{-d}, \quad -p \leq s \leq p \tag{17b}$$

$$I(s,V_o) = I_p + I_{-p} - I_{-d}, \quad -d \leq s \leq -p \tag{17c}$$

$$I(s,V_o) = I_p + I_{-p} - I_d - I_{-d}, \quad s \leq -d. \tag{17d}$$

Reduced Variable Formulation

The deflection of a thermal beam of alkali metal atoms should be described by Eq. (16) (assuming negligible detector width) as all the

particles of the beam will experience the same force. The deflection of a beam of alkali halides is far more complex however due to the distribution in rotational states and consequent distributions in the transverse force. In this case, part of the signal recorded on a detector of infinitesimal width at the position s would have arrived at the position s_o in the absence of an applied potential V_o and is characterized by a rotational energy W_r and $q = \cos\phi = M_J/_J$, that is

$$dI(s,V_o)ds = f(s_o)ds_o\rho(v)dv\rho(W_r,q)dW_r dq \tag{18}$$

where $\rho(W_r,q)dW_r dq$ is the probability of finding W_r and q in the intervals W_r to $W_r + dW_r$ and q to q + dq and $\rho(v)dv$ is the probability of finding the particle velocity along the field axis in the range v to v + dv. Then the total deflected signal arriving at s may be evaluated by first integrating over $f(s_o)$ and $\rho(v)$, yielding

$$I(s,V_o) = \int dW_r dq\rho(W_r,q)\int ds_o f(s_o)\rho(v)\left(\frac{\partial v}{\partial s}\right)_{s_o,\ W_r,\ q} \tag{19a}$$

or by first integrating over the thermal distributions to obtain

$$I(s,V_o) = \int ds_o f(s_o)\int dv dq\rho(v)\rho(W_r,q)\left(\frac{\partial W_r}{\partial s}\right)_{s_o,v,q}. \tag{19b}$$

Expression (19a) may be written as

$$I(s,V_o) = \int_0^\infty\int_{q_1}^{q_2} dW_r dq\rho(W_r,q)I(s,V_o;W_r,q). \tag{20}$$

For $s_\alpha(W_r,q,V_o) > 0$, $q_1 = 1/\sqrt{3}$, $q_2 = 1$, and $I(s,V_o;W_r,q)$ will be given by Eq. (16); when $s_\alpha(W_r,q,V_o) < 0$, the limits become $q_1 = 0.0$, $q_2 = 1/\sqrt{3}$, with $I(s,V_o;W_r,p)$ given by Eq. (17). Eq. (20) is still quite general; it assumes a thermal distribution in velocity and a field free profile given by Eq. (12), but leaves the functional form of $\rho(W_r,q)$ and

$s_\alpha(W_r, q, V_o)$ unspecified. In considering the deflection of beams with arbitrary distributions in W_r and q, Eq. (20) will prove the more fruitful approach. In fact, for some forms of the rotational distributions, part of the integral in Eq. (20) may be evaluated. Thus, as shown in Appendix B, the integral over $\cos\phi = q$ may be evaluated for an assumed isotropic distribution.

However, in considering the deflection of a beam with a thermal distribution in W_r and q,

$$\rho(W_r, q)dW_r dq = e^{-W_r/kT_r} d\left(\frac{W_r}{kT_r}\right) dq \tag{21}$$

where $0 < W_r < \infty$, $0 < q < 1$, it is easier to first integrate over W_r and q. The thermal distribution in flux velocities is given by

$$\rho(v)dv = 2\,\frac{v^3}{\alpha^4}\, e^{-v^2/\alpha^2} dv \tag{22}$$

where α is the most probable source velocity. In order to evaluate Eq. (19b), we define a reduced deflection, rotational energy, and translational energy by

$$\sigma = (s - s_o)/s_\alpha^o \tag{23a}$$

$$x = W_r/kT_r \tag{23b}$$

$$y = W_t/kT_t \tag{23c}$$

where T_r and T_t are the rotational and translational temperatures in degrees Kelvin ($T_r = T_t$ for a thermal beam) and

$$s_\alpha^o = \frac{\mu^2 E \frac{\partial E}{\partial z} L_1(L_1+2L_2)}{8k^2 T_r T_t} \tag{24}$$

is the deflection of the dipole for which $W_r = kT_r$, $|q| = 1$, and $v = \alpha$.

Following Frazer[25], it is possible to reduce Eq. (19b) to the following form:

$$I(s,V_o) = \int_{\sigma_1}^{\sigma_2} f(s-s_\alpha^o\sigma)W(\sigma)d\sigma \qquad (25)$$

where $\sigma_1 = \frac{s+d}{s_\alpha^o}$, $2 = \frac{s-d}{s_\alpha^o}$

and $W(\sigma) = \int_{q_1}^{q_2}\int_{}^{\infty} e^{-\frac{3q^2-1}{2\sigma y}} \frac{3q^2-1}{2y\sigma^2} e^{-y} y dy dq.$ (26)

where $q_1 = \frac{1}{\sqrt{3}}$, $q_2 = 1$ for $\sigma > 0$, $q_1 = 0$, $q_2 = \frac{1}{\sqrt{3}}$ for $\sigma < 0$. Physically $W(\sigma)d\sigma$ is the probability flux in the region σ to $\sigma + d\sigma$ measured on an infinitely narrow detector and originating by the deflection of an infinitely thin beam. The function $I(s,V_o)$ in Eq. (25) is still a relative flux normalized such that $\int_{-\infty}^{\infty} I(s,V_o)ds = p + d$.

The transmission of the field, the relative signal recorded at an applied potential V_o with the detector positioned at the center of the undeflected beam, is given by Eq. (25) as:

$$I(0,V_o) = \int_{\sigma_1}^{\sigma_2} f(-s_\alpha^o\sigma)W(\sigma)d\sigma.$$

Thus, the transmission of the field is a function only of s_α^o which for constant experimental geometry may be expressed as

$$s_\alpha^o \propto \frac{\mu^2 V_o^2}{T_t T_r}.$$

Assuming the product MX to be characterized by rotational and translational temperatures T_r and T_t, and assuming T_t to have been measured, comparison of the product MX transmission with that obtained with a

thermal calibration beam (reported in the next section) determines the rotational temperature of the product MX.

PRELIMINARY BEAM EXPERIMENTS

Deflection of Thermal Alkali Atoms

The deflection experienced by a thermal beam of cesium atoms upon traversing the field is shown in Fig. 11. Cesium atoms were chosen as a thermal test case because their large polarizability insured an easily measurable deflection and because the Cs_2 content of the beam should be negligible. The experimental distributions at 0 kv and 30 kv were measured on a hot tungsten wire 0.0076 cm in diameter. The two calculated deflection patterns shown in Fig. 11 as the solid and dashed curves were computed by Eq. 16. Accordingly, the calculations assumed negligible detector width, a thermal effusive distribution in velocities, a constant force over the dimensions of the beam, and a zero field beam profile described by Eq. 12 with p = 0.005 cm and d = 0.043 cm (shown as the dash-dot-dash curve of Fig. 11).

It was not possible to calculate $I(s,30)$ without first determining the value of z at which the beam traverses the field, and thereby determining the ratio $E(\partial E/\partial z)/V_o^2$. The experimental deflection of cesium atoms could be used to calculate z by varying s_α and therefore $E(\partial E/\partial z)/V_o^2$ until obtaining the best fit between the experimental and calculated deflection patterns. However, as described later, a more precise value of z was obtained by comparing the experimental and theoretical deflection of a thermal cesium chloride beam; this calculation led to a best

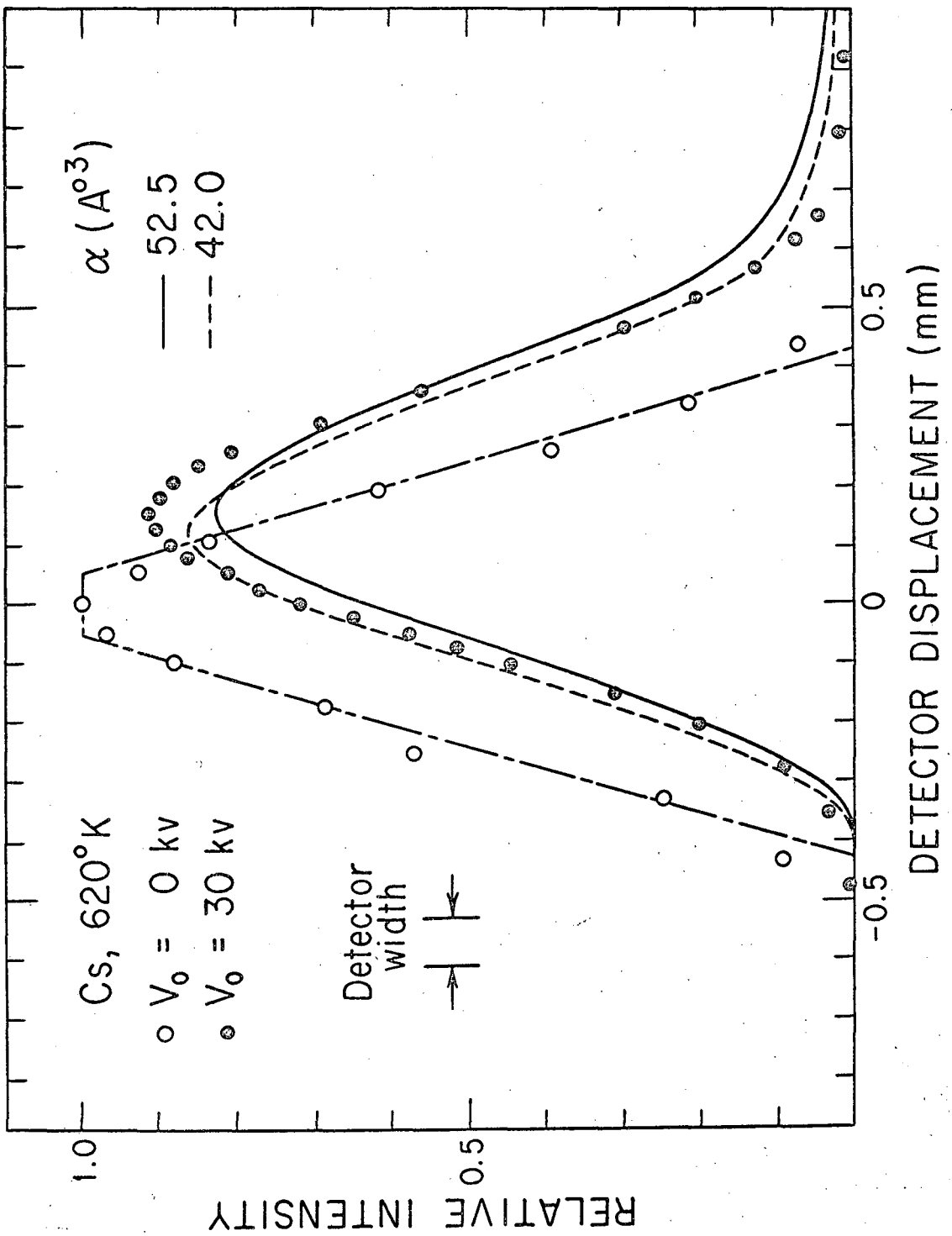

Fig. 11. Deflection of a thermal cesium atom beam. The experimental deflection patterns are compared with those predicted from Eq. (16).

value of z/a of 1.51 implying that for our experimental geometry:

$$E = 2.97\ V_o \quad (v/cm) \tag{27a}$$

$$\frac{\partial E}{\partial z} = -8.63\ V_o \quad (v/cm^2) \tag{27b}$$

and

$$E\,\frac{\partial E}{\partial z} = -25.6\ V^2 \quad (v^2/cm^3)$$

where V_o is measured in volts.

Thus, at 30 kilovolts, taking Salop, Pollack and Bederson's value[31] for the cesium polarizability of 52.5 $\mathring{A}^3$, and employing the working formula cited in Table II, a dipole moment of

$$\mu_\rho = (3.3356\times10^{-9})\ (52.5)\ (2.97)\ (3\times10^{4}) = 0.0156 \text{ Debyes}$$

should be induced in the cesium atoms, resulting in a deflection of the most probable source velocity of $s_\alpha = 0.24$ mm. A plot of $I(s,30\text{ kv})$ calculated from Eq. (16) for $s_\alpha = 0.24$ mm is shown as the solid curve in Fig. 11. The dashed curve of Fig. 11 was calculated for $s_\alpha = 0.20$ mm, corresponding to a cesium polarizability of 42 $\mathring{A}^3$; this is the lower limit of the range of values quoted by Chamberlain and Zorn[32] and is also the value found by Scheffers and Stark[33] in an early electric deflection measurement.

Neither calculated curve can be said to be in good agreement with the experimental one. The peak position of the solid curve matches well with the experimental values, while the dashed curve seems to match intensity and overall curve shape better. Indeed, from the two calculated curves, it is apparent that no value of s_α will make $I(s,30\text{ kv})$ coincide with the experimental curve. Consequently, in order to obtain more quantitative agreement between the calculated and experimental

deflection patterns, it would probably be necessary to incorporate into the calculation the detector width, experimental field free beam profile, variation in F_z over the dimensions of the beam, and possibly deviations in the velocity distribution from the Boltzmann flux distribution.

Incorporation of the experimental detector width in the calculations would round off the corners on the theoretical zero field profile; it would probably have much less effect on the shape of the thirty kilovolt patterns except that the peaks would be slightly flatter and broader. As remarked previously F_z will show only a slight dependence on y over the height of the beam. However, the beam width will introduce an uncertainty in z on the order of $|\Delta z/a| \sim .08$. Thus, the assumption of a constant force, F_z, over the width of the beam will probably result in an experimental distribution skewed to high field with respect to the calculated distribution.

The experimental points at zero field shown in Fig. 11 do not fall to zero as fast as theoretically predicted. While part of this effect is due to the finite width of the detector, it is almost certainly due as well to scattering of the beam traversing the field by background gas. The cold shield between S_1 and S_2 shwon in Fig. 3 was installed to reduce this effect. During experiments measuring product alkali halide deflections prior to installation of this cold shield, appreciable R-X scattering gas entered the region between S_1 and S_2, thereby extensively broadening the beam arriving at the detector. Finally, even in this experiment measuring the deflection of a cesium beam effusing from a thermal source, the actual velocity distribution may

not accurately obey a thermal distribution. There may well be a distortion, especially pronounced at low velocities, due to Cs-Cs scattering within the beam. In fact, Chamberlain and Zorn[32] remark that their experimental distribution is somewhat broader than that they calculate. While they did not really know the cause of this broadening, they suggest that it may be due to cesium-cesium scattering within the beam, thereby altering the velocity distribution.

Deflection of a Thermal Cesium Chloride Beam

Cesium chloride was chosen as a thermal calibration standard because it does not associate into dimers to a detectable extent in the gas phase[34]. The transmission of the field, $I(0,V_o)$ for a thermal CsCl beam is plotted versus applied potential in Fig. 12. One adjustable parameter, the experimental value of z/a, was varied to obtain the best fit between the experimental values and those calculated by numerical integration over $W(\sigma)$ employing a step size in s_o of 0.0002 cm. The characteristic deflection of the beam, s_α^o of Eq. (24), was varied by varying the parameter $-E(\partial E/\partial z)/V_o^2$ in order to obtain the best fit. The function $W(\sigma)$ has been calculation by Feierabend[26] by numerical integration and is plotted in Fig. 13. This best fit between experimental and calculated values was obtained for $z/a = 1.51$; thus, E and $\partial E/\partial z$ are related to V_o in the experiments described in this report as expressed in Eq. (27). The fact that the experimental transmissions become higher than that calculated at high fields is probably due to the fact that the field free distribution did not experimentally fall to zero as fast as $f(s_o)$ would predict, probably for the reason mentioned earlier

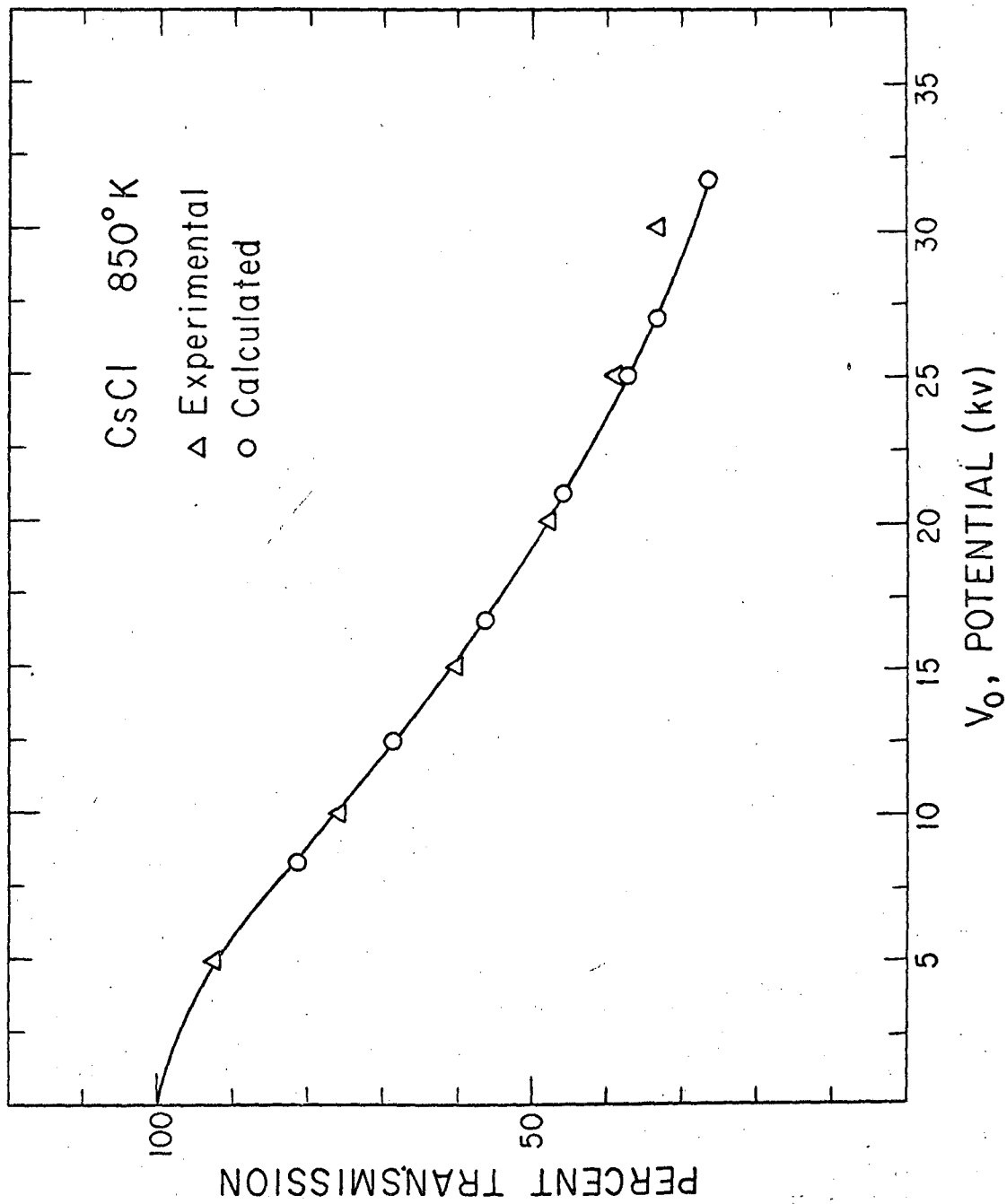

Fig. 12. Experimental and calculated transmission for a thermal cesium chloride beam.

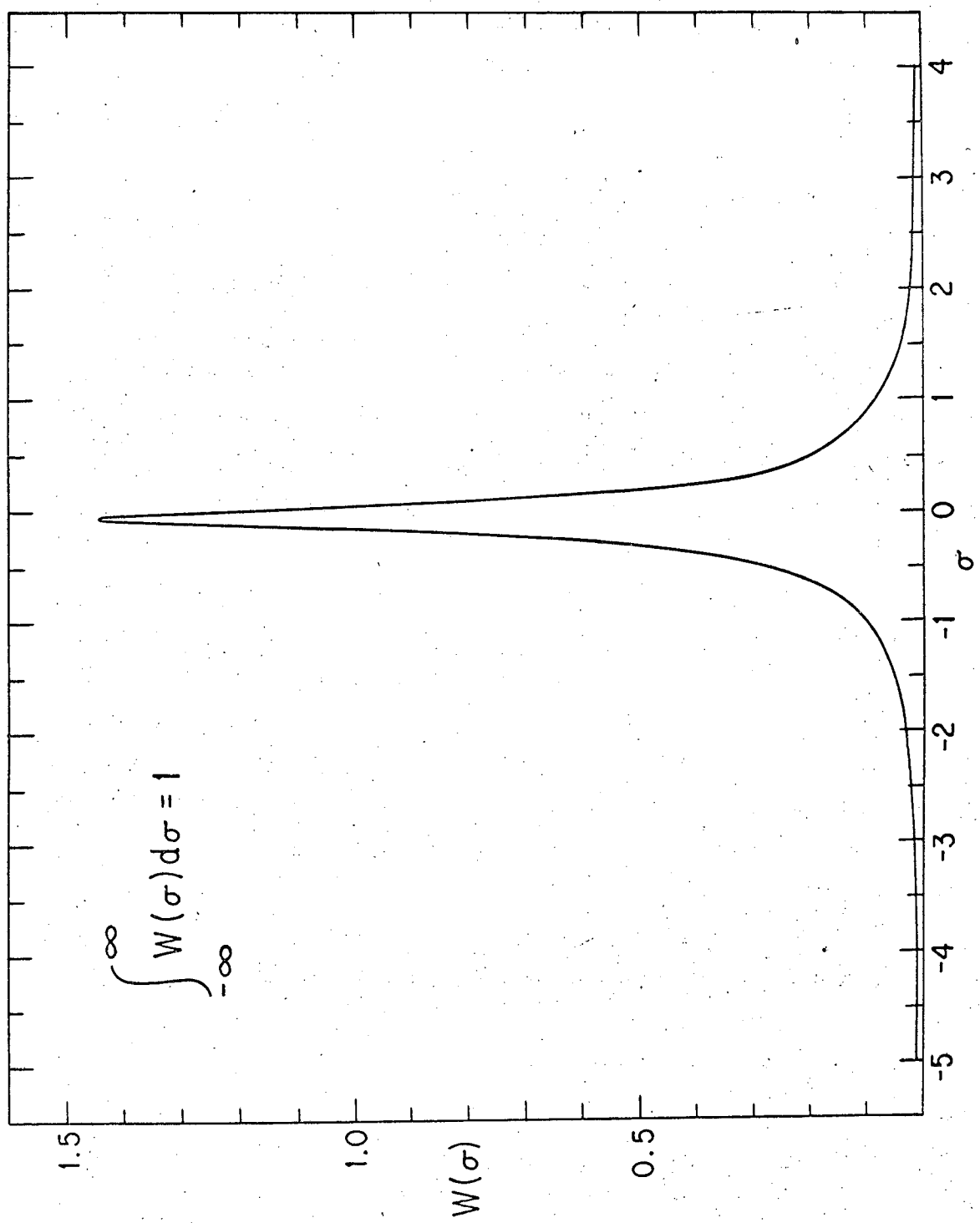

Fig. 13. Plot of W(σ) of Eq. (26) versus σ derived from calculations of Feierabend.[26]

(Fig. 14 shows the experimental shape of $f(s_o)$). Furthermore, it was not possible to calculate the transmission at low field from Eq. (25), as values of $W(\sigma)$ are required for $|\sigma|$ in excess of the range tabulated by Feiserabend. The fact that contributions from large σ can be important is dramatized by the fact that $\omega(\sigma)$ is defined such that $\int_{-\infty}^{\infty} \omega(\sigma)d\sigma = 1$, whereas integration over the range of σ tabulated by Feiserabend yields $\int_{-5}^{4} \omega(\sigma)d\sigma = 0.901$.

Fig. 14 compares the deflection pattern produced at 15 kv by a thermal cesium chloride beam with that calculated by numerical integration of Eq. (25) with a step size in s_o of 0.0007 cm. Once again the calculated relative signal, $I(s,V_o)$, is too low at large s ($|s| > \sim 0.4$ mm) because experimentally $f(s_o)$ does not fall to zero as fast as assumed for the calculation. The width of the experimental zero-field curve also appears to be narrower than that assumed. Finally, the experimental curve appears to be shifted slightly with respect to that calculated toward the high field region. Incorporation of a small polarizability interaction into the calculation would probably account for this. Thus, a polarizability of 6.2 Å^3 for CsCl would result in an s_α of 0.03 mm, as calculated from the formulae in Table II; this is roughly the distance the calculated pattern needs to be shifted in order that it be symmetrically placed about the experimental pattern.

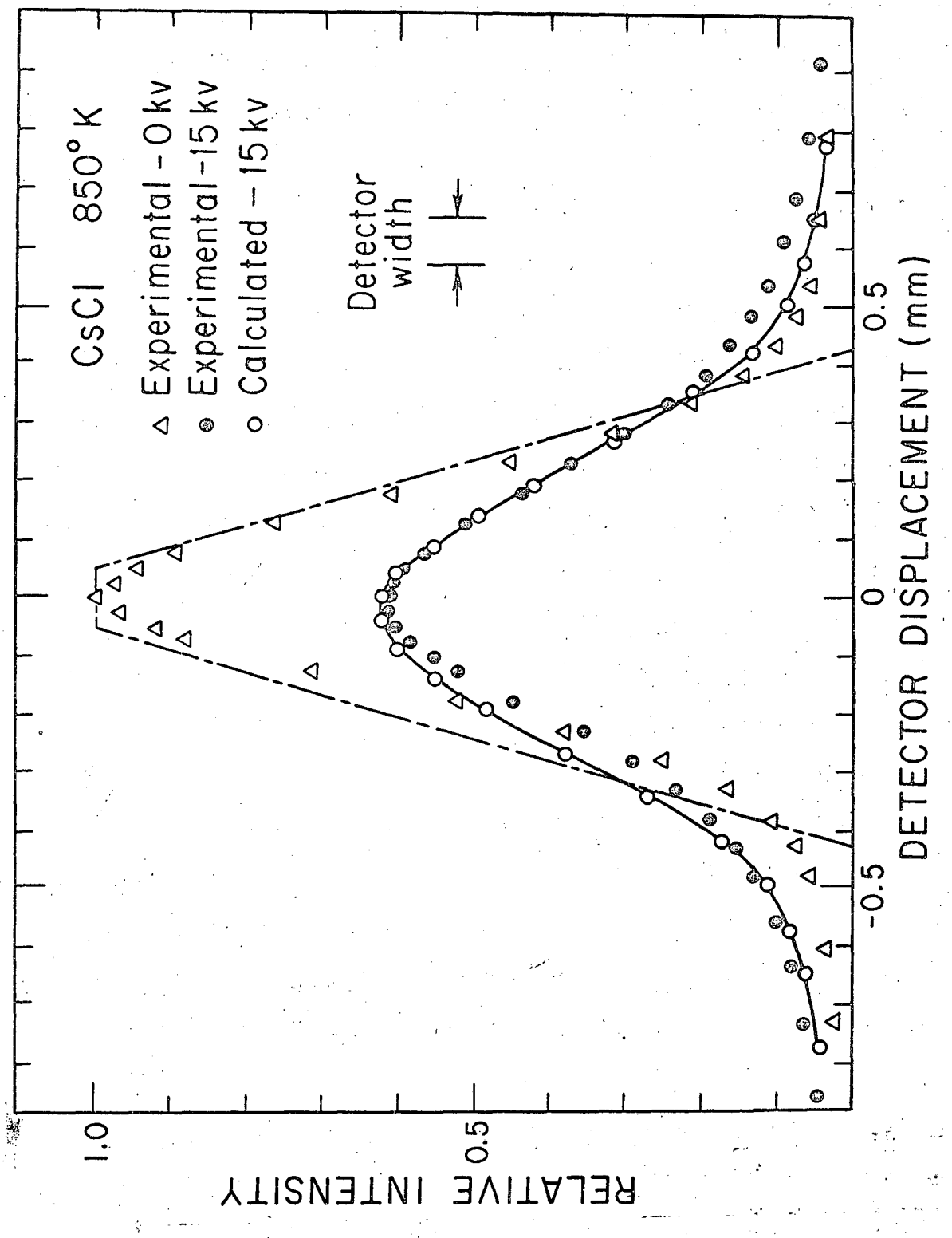

Fig. 14. Experimental and theoretical deflection patterns for a thermal cesium chloride beam.

APPENDIX A

Properties of Alkali Metals and Alkali Halides

Relevant properties of the alkali metals and alkali halides are summarized in this appendix in the form of three tables. Most of the entries in these tables are self-explanatory, although a few warrant additional discussion here.

Table AI lists relevant properties of the alkali metals. Salop, Pollack and Bederson[31] measured the alkali atom polarizabilities by means of the "E-H gradient Balance" method. By employing pole tips which were simultaneously electric and magnetic equipotentials of the "two-wire[19] configuration, they achieved congruent electric and magnetic fields in the gap. By balancing the magnetic and electrical interactions on a beam of alkali metals traversing the field and subsequently determining the values of H and E, they measured the polarizabilities with a minimum of experimental errors. Chamberlain and Zorn's[32] values of the alkali metal polarizabilities are included in Table AI because they are the most recent measurements obtained by observing the deflection of the beam in an inhomogeneous electric field, the same method being described here. There appear to be no measurements of the polarizability of the alkali metal dimers. A number of useful properties of the alkali halides have been listed in Table AIII. The masses listed refer to the natural isotopic abundances; the isotopic identification indicates the particular isotope to which the quoted rotational constant refers (these numbers are known to many more figures than are indicated here[35]). The polarizabilities were estimated on a model of the alkali halide molecule as two charged

spheres. The polarizability was assumed spherical ($\alpha_{xx} = \alpha_{yy} = \alpha_{zz}$) and was taken as the sum of the polarizabilities of the appropriate alkali and halogen ions. These ionic polarizabilities were in turn taken from Rittner[36] and were initially calculated by Pauling.[37] Again, there do not appear to be any experimental measurements of these polarizabilities.

Table AI. POLARIZABILITIES OF ALKALI ATOMS

Metal	Mass (gm/mole)	α-Polarizability ($Å^3$) Salop, et al[a]	Chamberlain and Zorn[b]
Li	6.95	20 ± 3	22 ± 2
Na	22.99	20 ± 2.5	21.5 ± 2
K	39.10	36 ± 4.5	38 ± 4
Rb	85.48	40 ± 5	38 ± 4
Cs	132.91	52.5 ± 6.5	48 ± 6

[a] Reference 31.

[b] Reference 32.

Table AII. PROPERTIES OF ALKALI DIMERS[a]

Dimer	Mass (gm/mole)	D_o^o (kcal/mole)	$\log_{10} Kp = \log_{10} Pm/Pd^2$ (atm)	r_m (Å)	B (cm^{-1})	ω_e (cm^{-1})
Li_2	13.88	25.76 ± .10	16.9304	2.672	0.67272	351.43
Na_2	45.98	17.53 ± .15	10.3780	3.078	0.15471	159.23
K_2	78.20	11.85 ± .10	6.09178	3.923	0.05622	92.64
Rb_2	170.96	11.30 ± .30	5.7032	4.12	0.0231	57.28
Cs_2	265.82	10.38 ± .30	5.0623	4.46	0.0127	41.99

[a] W. H. Evans, R. Jacobson, T. R. Munson, and D. D. Wagman, J. Research Nat'l Bureau Standards 55, 83 (1955).

Table AIII. PROPERTIES OF ALKALI HALIDES

	Mass M (gms/mole)	Polarizability[a] α ($Å^3$)	Dipole Moment μ (Debye)	Rotational[b] Constant B (cm^{-1})	Vibrational frequency ω_e (cm^{-1})
Li^6F	25.94	1.1	6.6[c]	1.5087	906.2[i]
Li^7Cl^{35}	42.40	3.7	7.12[b]	0.7065	662[g]
Li^7Br^{79}	86.86	4.8	6.19[c]	0.5554	576[g]
Li^7I^{127}	133.85	7.2	6.64[c]	0.4432	501[g]
NaF	41.99	1.2	8.37[d]	0.4369	(463)[k]
$NaCl^{35}$	58.45	3.9	8.5[c]	0.2181	366[h]
$NaBr^{79}$	102.91	5.0	9.4[e]	0.1513	302[h]
NaI^{127}	149.90	7.3	(9.3)[f]	0.1178	258[h]
$K^{39}F$	58.10	1.9	7.33[c]	0.2799	400[j]
$K^{39}Cl^{35}$	74.56	4.5	10.48[c]	0.1286	281[h]
$K^{39}Br^{79}$	119.02	5.7	10.41[c]	0.0812	213[h]
$K^{39}I^{127}$	166.01	8.0	11.1[c]	0.0609	(173)[h]
$Rb^{85}F$	104.48	2.5	8.80[c]	0.2107	390[j]
$Rb^{85}Cl^{35}$	120.94	5.1	10.6[e]	0.0876	228[h]
$Rb^{85}Br^{79}$	165.40	6.2	10.5[e]	0.0475	(166)[h]
$Rb^{85}I^{127}$	212.39	8.6	(10.8)[f]	0.0328	(128)[h]
CsF	151.91	3.5	7.88[c]	0.1844	385[j]
$CsCl^{35}$	168.37	6.1	10.5[c]	0.0721	209[h]
$CsBr^{79}$	212.83	7.2	10.7[e]	0.0361	(139)[h]
CsI^{127}	259.82	9.6	12.1[c]	0.0236	(101)[h]

[a]Estimated as described in text.

[b]Reference 35.

[c]Reference 3.

[d]R. K. Bauer and H. Lew, Can. J. Phys. 41, 1461 (1963).

[e]A. L. McClellan, Tables of Experimental Dipole Moments (W. H. Freeman and Co., San Francisco and London, 1963).

[f]These are theoretical estimates; see reference 36.

[g]W. Klemperer and S. A. Rice, J. Chem. Phys. 26, 618 (1957).

[h]S. A. Rice and W. Klemperer, J. Chem. Phys. 27, 573 (1957).

[i]G. L. Vidale, J. Phys. Chem. 64, 314 (1960).

[j]R. F. Barrow and A. D. Cannt, Proc. Roy. Soc. (London) A219, 120 (1953).

[k]Y. P. Varshni, J. Chem. Phys. 28, 1081 (1958).

APPENDIX B

Transmission as a Function of W_r for an Isotropic M_J Distribution

In this appendix, an expression for the transmission through the electric field as a function of the rotational energy of the molecule W_r is evaluated for a beam of molecules charactered by a translational temperature T_t, a field free beam profile given by Eq. (12), and an isotropic distribution in M_J. The molecule is assumed to experience a second order Stark effect in the field. Then, the observed transmission through the field, $R(V_o)$, will be given in terms of the transmission of one rotation state, $R(W_r;V_o)$ by

$$R(V_o) = \sum_{W_r} \rho(W_r)R(W_r;V_o). \tag{B1}$$

The deflection of a particle travelling with the most probable source velocity α will be given in the classical limit where $\cos\phi = M_J/J$ by

$$s_\alpha = \frac{\gamma}{W_r} G, \tag{B2a}$$

where

$$G = \frac{3\cos^2\phi - 1}{4} \tag{B2b}$$

and

$$\gamma = \left| \frac{\mu^2 E \; \partial E/\partial z \;\; L_1(L_1+2L_2)}{4kT_t} \right|. \tag{B2c}$$

It is convenient at this point to define $R(W_r;V_o)$ as

$$R(W_r;V_o) = R^+(W_r;V_o) + R^-(W_r;V_o), \tag{B3}$$

where R^+ originates from particles suffering positive deflections and R^- from those suffering negative deflections (by convention $M_J/J > 1/\sqrt{3}$ results in positive deflections). The distributions in $M/J = \cos\phi = q$

is assumed isotropic so that the distribution in q is given by

$$\rho(q)dq = \frac{1}{2}dq, \quad -1 \leq q \leq 1. \tag{B4}$$

Consequently, from Eq. (16) assuming a negligible detector width we obtain

$$R^{+}(W_r;V_o) = \int_{\frac{1}{\sqrt{3}}}^{1} dq \left\{ \frac{d}{d-p} e^{-\frac{\gamma G(q)}{W_r d}} - \frac{p}{d-p} e^{-\frac{\gamma G(q)}{W_r p}} \right\} \tag{B5}$$

This may be evaluated in terms of the error function defined as[38]

$$\mathrm{erf}(z) = \frac{2}{\sqrt{\pi}} \int_0^z e^{-t^2} dt' \tag{B6}$$

the results are:

$$R^{+}(W_r;V_o) = \frac{W_r^{1/2}\sqrt{\pi}}{(d-p)\sqrt{3\gamma}} \left\{ d^{3/2} e^{\gamma/4W_r d} \left(\mathrm{erf}\left(\sqrt{\frac{3\gamma}{4W_r d}} \right) - \mathrm{erf}\left(\sqrt{\frac{\gamma}{4W_r d}} \right) \right) \right.$$

$$\left. - p^{3/2} e^{\gamma/4W_r p} \left(\mathrm{erf}\left(\sqrt{\frac{3\gamma}{4W_r p}} \right) - \mathrm{erf}\left(\sqrt{\frac{\gamma}{4W_r p}} \right) \right) \right\} . \tag{B7}$$

In a similar manner

$$R^{-}(W_r;V_o) = \int_0^{1/\sqrt{3}} dq \left\{ \frac{d}{d-p} e^{\frac{\gamma G(q)}{W_r d}} - \frac{p}{d-p} e^{\frac{\gamma G(q)}{W_r p}} \right\}. \tag{B8}$$

This may be evaluated in terms of Dawson's integral[38]

$$\mathrm{Daw}(z) = e^{-z^2} \int_0^z e^{t^2} dt; \tag{B9}$$

the results are:

$$R^{-}(W_r;V_o) = \frac{2W_r^{1/2}}{(d-p)\sqrt{3\gamma}} \left\{ d^{3/2} \mathrm{Daw}\left(\sqrt{\frac{\gamma}{4W_r d}} \right) - p^{3/2} \mathrm{Daw}\left(\sqrt{\frac{\gamma}{4W_r p}} \right) \right\}. \tag{B10}$$

References

1. N. F. Ramsey, Molecular Beams (Clarendon Press, Oxford, 1956), chapter 10.

2. K. F. Smith, Molecular Beams (Methuen Monographs, 1955).

3. P. Kusch and V. V. Hughes, in Handbuch der Physik (Springer-Verlag, Berlin, 1959), Vol. 37/1.

4. H. G. Bennewitz, K. H. Kramer, W. Paul, and J. P. Toennies, Z. Physik 177, 84 (1964).

5. K. H. Kramer and R. B. Bernstein, J. Chem. Phys. 42, 767 (1965).

6. "Electric Deflection of Atomic and Molecular Beams" by D. R. Herschbach in Inorganic Materials Research Division Annual Report, 1962, UCRL Report 10706 (University of California Radiation Laboratory, Berkeley, February, 1963).

7. R. R. Herm and D. R. Herschbach, J. Chem. Phys., (to be published).

8. D. R. Herschbach, The Vortex 22, 348 (1961).

9. N. C. Blais and D. L. Bunker, J. Chem. Phys. 37, 2713 (1962); D. L. Bunker and N. C. Blais, J. Chem. Phys. 41, 2377 (1964).

10. M. Karplus and L. M. Raff, J. Chem. Phys. 41, 1267 (1964).

11. P. Pechukas, J. C. Light, and C. Rankin, J. Chem. Phys., (to be published).

12. For a discussion of focussing electric fields see: H. G. Bennewitz, W. Paul, and Ch. Schlier, Z. Physik 141, 6 (1955).

13. U. von Zahn, Rev. Sci. Instr. 34, 1 (1963).

14. W. Paul, H. P. Reinhard, and U. von Zahn, Z. Physik 152, 143 (1958).

15. E. McMillan, Phys. Rev. 38, 1568 (1931).

16. J. A. Norris, UCRL Report 10848 (University of California Radiation Laboratory, Berkeley, June 1963).

17. K. R. Wilson, UCRL Report 11605 (University of California Radiation Laboratory, Berkeley, August, 1964).

18. H. K. Hughes, Phys. Rev. 72, 614 (1947).

19. I. I. Rabi, J. M. B. Kellog, and J. R. Zacharias, Phys. Rev. 46, 157 (1934).

20. For detailed discussions of the "two-wire field" as an electric or magnetic inhomogeneous deflecting field see references 1 and 3.

21. For a description of an inhomogeneous "two-wire" electromagnet which we have also constructed for use in scattering experiments see: R. R. Herm and D. R. Herschbach, UCRL Report 10526 (University of California Radiation Laboratory, Berkeley, October, 1962).

22. A. J. Hebert, UCRL Report 10482 (University of California Radiation Laboratory, Berkeley, September, 1962).

23. For a discussion of the behavior of the platinum filament under operating conditions see: K. R. Wilson, G. H. Kwei, J. A. Norris, R. R. Herm, J. H. Birely, and D. R. Herschbach, J. Chem. Phys. 41, 1154 (1964).

24. High Voltage Standard Type Power Pack HV 500-502, manufactured by Plastic Capacitors, Inc., 2620 N. Clylowen Avenue, Chicago 14, Ill.

25. S. Datz, D. R. Herschbach, and E. H. Taylor, J. Chem. Phys. 35, 1549 (1961).

26. R. G. J. Frazer, Molecular Rays (Cambridge University Press, Cambridge, 1931), chapter 6.

27. L. Wharton, M. Kaufman, and W. Klemperer, J. Chem. Phys. 37, 621 (1962). We have corrected a typographical error in their formula for A.

28. S. A. Marshall and J. Weber, Phys. Rev. 105, 1502 (1957).

29. Reference 1, pp. 16-18.

30. Reference 1, pp. 92-100.

31. A. Scalop, E. Pollack, and B. Bederson, Phys. Rev. 124, 1431 (1961).

32. G. E. Chamberlain and J. C. Zorn, Phys. Rev. 129, 677 (1963).

33. H. Scheffers and J. Stark, Z. Physik 35, 625 (1934).

34. Measurements of the dimerization of alkali halides in the gas phase have been made by: (a) R. C. Miller and P. Kusch, J. Chem. Phys. 25, 860 (1956); Erratum, J. Chem. Phys. 27, 981 (1957); (b) S. Datz, W. T. Smith, Jr., and E. H. Taylor, J. Chem. Phys. 34, 558 (1961); (c) The available data on monomer-dimer equilibrium is summarized by: L. Brewer and E. Brackett, Chem. Revs. 61, 425 (1961).

35. D. R. Lide, Jr., P. Cahill, and L. P. Gold, J. Chem. Phys. 40, 156 (1964).

36. E. S. Rittner, J. Chem. Phys. 19, 1030 (1951).

37. L. Pauling, Proc. Roy. Soc. (London) A114, 191 (1927).

38. These integrals are tabulated in: M. Abramowitz and I. A. Stegum, Handbook of Mathematical Functions (National Bureau of Standards Applied Mathematics Series 55, 1965).